2

Titan's surface geology

O. AHARONSON, A. G. HAYES, P. O. HAYNE, R. M. LOPES, A. LUCAS, AND J. T. PERRON

2.1 Overview

The presence of an atmosphere, initially suggested based on limb darkening by Sola (1904) and later by the presence of methane spectral lines by Kuiper (1944), has long given Titan a special place in the minds of planetary geologists. The first close-up images were obtained by Pioneer 11 in 1979 (Gehrels et al., 1980), confirming a substantial atmosphere. These early observations led to the diversion of the trajectory of the *Voyager I* spacecraft to a closer encounter with Titan in 1980. Although the visible cameras on *Voyager* also had difficulty seeing Titan's surface (Richardson et al., 2004), radio occultation experiments suggested a surface pressure of 1.5 bars and temperature near 95 K (Lindal et al., 1983). These results were exciting because, for a methane mixing ratio of a few percent at the surface (Hunten, 1978), they placed methane's partial pressure near its triple point. Thus, like water on Earth, solid, liquid, and gaseous methane could potentially exist in Titan's environment. Ethane, which is the main product of methane photolysis, can also be liquid under these conditions. The presence of condensable volatiles in Titan's thick atmosphere opens the door for active fluvial, lacustrine, and pluvial processes that can shape its landscape with similar morphologies to those we find on Earth.

Prompted by the exciting results of the *Voyager* mission and the nearly two decades of Earth-based imaging campaigns that followed, NASA/ESA launched the *Cassini-Huygens* mission to Saturn in 1997. To penetrate Titan's thick atmosphere, *Cassini* is equipped with a Ku-band radar capable of obtaining images of the surface at a scale of 300 meters. *Cassini's* instrument suite also includes the Imaging Science Subsystem (ISS) and Visual and Infrared Mapping Spectrometer (VIMS), which are imaging systems that operate at visible and infrared wavelengths. These instruments can see down to the surface by utilizing windows in the methane absorption spectrum, with resolution ranging from 200 m to 15 km.

The 2004 arrival of the *Cassini* spacecraft to Saturn's system has ushered in a new era in studying Titan. Its instrument suite has shed light on a group of landforms and processes that mirror those on Earth with surprising richness. The appearance and distribution of the morphologic units, and the interplay among the associated geologic processes, are important for constraining models of the interior, surface-atmosphere interactions, climate, and landscape/climate evolution.

In reviewing these recent discoveries, the focus here will be first on the geologic units mapped from orbit, and subsequently on the processes deduced to govern their evolution. Titan's surface is morphologically sculpted by a rich variety of aeolian, pluvial, fluvial, lacustrine, tectonic, impact, and possibly cryovolcanic processes. These processes are found to be directly analogous to those that shape Earth's surface. Both Titan and Earth have wind, rain, evaporation, erosion, standing bodies of liquid, and a subsurface hydrology.

As Titan's atmosphere is transparent to microwave radiation and synthetic aperture radar (SAR) images are of the highest resolution (up to 300 m/pixel) available globally, these data are particularly useful for mapping purposes (Lopes et al., 2010). Radar backscatter variations in SAR images can be interpreted in terms of variations of surface slope at the pixel scale, near-surface roughness at the wavelength scale, subsurface structure the scale of the penetration depth (~1–10 m for Titan-relevant materials), and near-surface dielectric

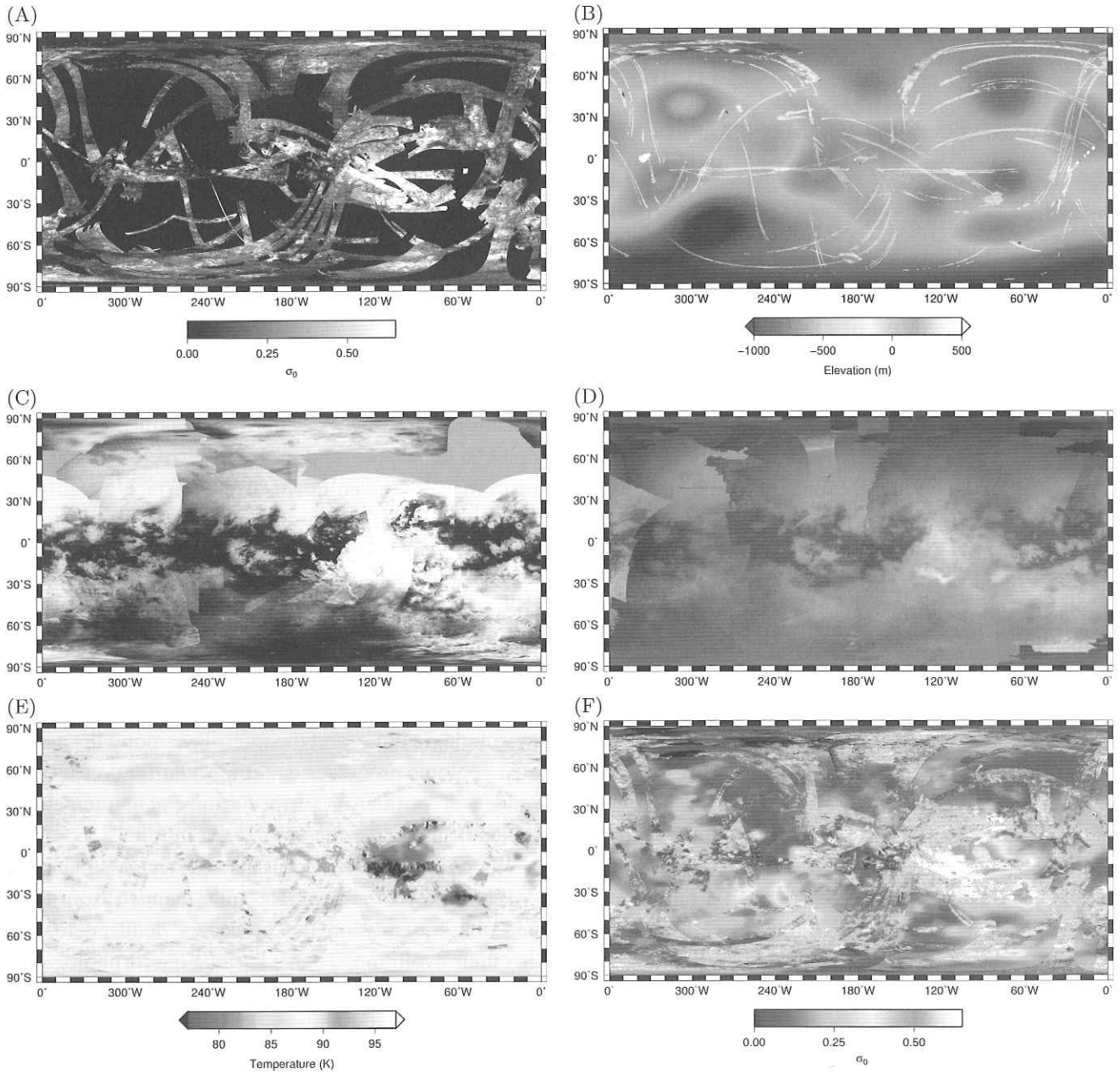

Figure 2.1 Global mosaics of Titan surface data sets, including (A) SAR images, (B) topography derived from altimetry, SAR-topo and stereo techniques (Zebker et al., 2009; Kirk et al., 2007; Stiles et al., 2009), (C) ISS images (NASA PIA13908), (D) VIMS false-color mosaic using reflectance at 5.0 (red), 2.0 (green), and 1.3 (blue) microns wavelength (adapted from Barnes et al. (2009b), (E) RADAR radiometry (Janssen et al., 2010), and (F) RADAR scatterometry (Zebker et al., 2008). (See color plate.)

properties. On Titan, the candidate surface materials (e.g., water ice, water-ammonia ice and other mixtures, hydrates, hydrocarbons, and tholins) are different from the rocky surfaces typically imaged with terrestrial radars; in particular, volume scattering at Titan is found to be significant (e.g., Janssen et al., 2009) due to lower attenuation and greater penetration depth.

The RADAR instrument on board *Cassini* (Elachi et al., 2004) operates in multiple modes, as an imaging SAR, an altimeter, a radiometer, and a scatterometer (Figure 2.1A, B, E, F, respectively). In addition to direct altimetry measurements, innovative data processing techniques have been used to derive topography. Stereogrammetry techniques have been developed that use overlapping SAR swaths to create digital elevation

models (DEMs) (Kirk et al., 2007), and a relatively new technique known as SAR Topo (Stiles et al., 2009) makes use of the overlap between the instrument's five beams and their relative returns. Initial comparisons among altimetry, stereo, and SAR-Topo have shown promising correlations among the various techniques (Stiles et al., 2009). SAR-Topo strips are available for nearly every SAR swath and provide a sparsely populated map of global topography (Zebker et al., 2009). Recent work has focused on reducing the speckle noise in SAR images to improve the usage of the data (Lucas et al., 2011) based on the work of Deledalle et al. (2009).

Titan's surface is almost completely obscured by the atmosphere at visible wavelengths. However, *Cassini's* ISS is equipped with a 0.938 μm narrow band pass filter and infrared polarizing filters that take advantage of a window in the methane's absorption spectrum and the high polarization of haze at phase angles near 90° (West and Smith, 1991; Porco et al., 2004). Images are acquired with wide- and narrow-angle cameras over the wavelength range from 200 to 1100 nm (Figure 2.1C). The VIMS instrument (Brown et al., 2004) operates in the spectral range 0.35 to 5.2 μm and can image the surface in windows centered at 0.94, 1.08, 1.28, 1.6, 2.0, 2.8, and 5.0 μm, where Titan's atmosphere is nearly transparent (Barnes et al., 2007). Reflectance spectra are used to derive and map compositional units. The resolution of Titan observations acquired by these cameras, which is hindered by atmospheric scattering and absorption, varies with both the distance of the spacecraft and observational geometry. ISS spatial resolution ranges from 1 to 10 km, with relatively small areas imaged at 1 km/pixel. VIMS resolution ranges average a few km/pixel but for small areas can be as high as 250 m/pixel (Jaumann et al., 2009b). The atmospheric effects require correlations to determine surface composition.[1]

The *Huygens* descent imager/spectral radiometer (DISR) (Tomasko et al., 2002; Tomasko et al., 2005) provided images of the landing site at resolutions unattainable from orbit, ranging from tens to hundreds of meters during descent down to centimeters upon touchdown. These data have proven particularly valuable for illuminating Titan's fluvial geology, as described later. Various physical properties of the surface were measured by instruments on *Huygens*. The probe provided information constraining soil properties at the landing site (10°S, 192°W) and suggested the presence of a damp porous medium consisting of loosely packed particles between the sizes of silt and medium sand (Lorenz et al., 2006a; Zarnecki et al., 2005). Data from the gas chromatograph-mass spectrometer (GCMS) instrument (Niemann et al., 2002) following touchdown provided evidence for release of both methane and ethane, as well as propane, acetylene, cyanogen, and carbon dioxide from the regolith beneath the probe (Lorenz et al., 2006b; Niemann et al., 2010).

[1] When describing remote sensing observations from the *Cassini* orbiter, images may be assigned TN or RevN designations. TN is the *Cassini* project acronym that refers to the Nth Titan encounter. RevN is the *Cassini* project designation referring to the spacecraft Nth revolution around Saturn. RevN designations are typically used for ISS images acquired during non-targeted encounters of Titan.

2.2 Global geologic units

Data from multiple instruments on board the *Cassini* spacecraft are used to map and classify distinct surface morphologies to determine possible emplacement sequences and mechanisms and the overall distribution of geologic processes on Titan. These data sets have revealed a wide variety of morphologic features, examples of which are shown in Figure 2.2. These characteristic terrain types are representative of the widely distributed geologic units found on Titan. Figure 2.3 shows the global distribution of these mapped units. Unit definitions and distributions, based on Lopes et al. (2010), are presented in the text that follows. The geologic processes that are thought to have created these morphologic units are discussed in the following sections.

Hummocky and mountainous terrain unit: these features consist of numerous patches of radar-bright, textured terrains, some of which have been interpreted to be of tectonic origin (Radebaugh et al., 2007). Among these features are elongated mountain chains, ridge-like features, elevated blocks that stand generally isolated, and bright terrains of a hilly or hummocky appearance (Figure 2.2(B)). This terrain is found mostly as isolated patches or long mountain chains, small in areal extent. The exception is Xanadu (Figure 2.2(A)), which Lopes et al. (2010) classified as a sub-unit of the hummocky and mountainous terrain unit. Where available, topographic profiles show that these features are elevated

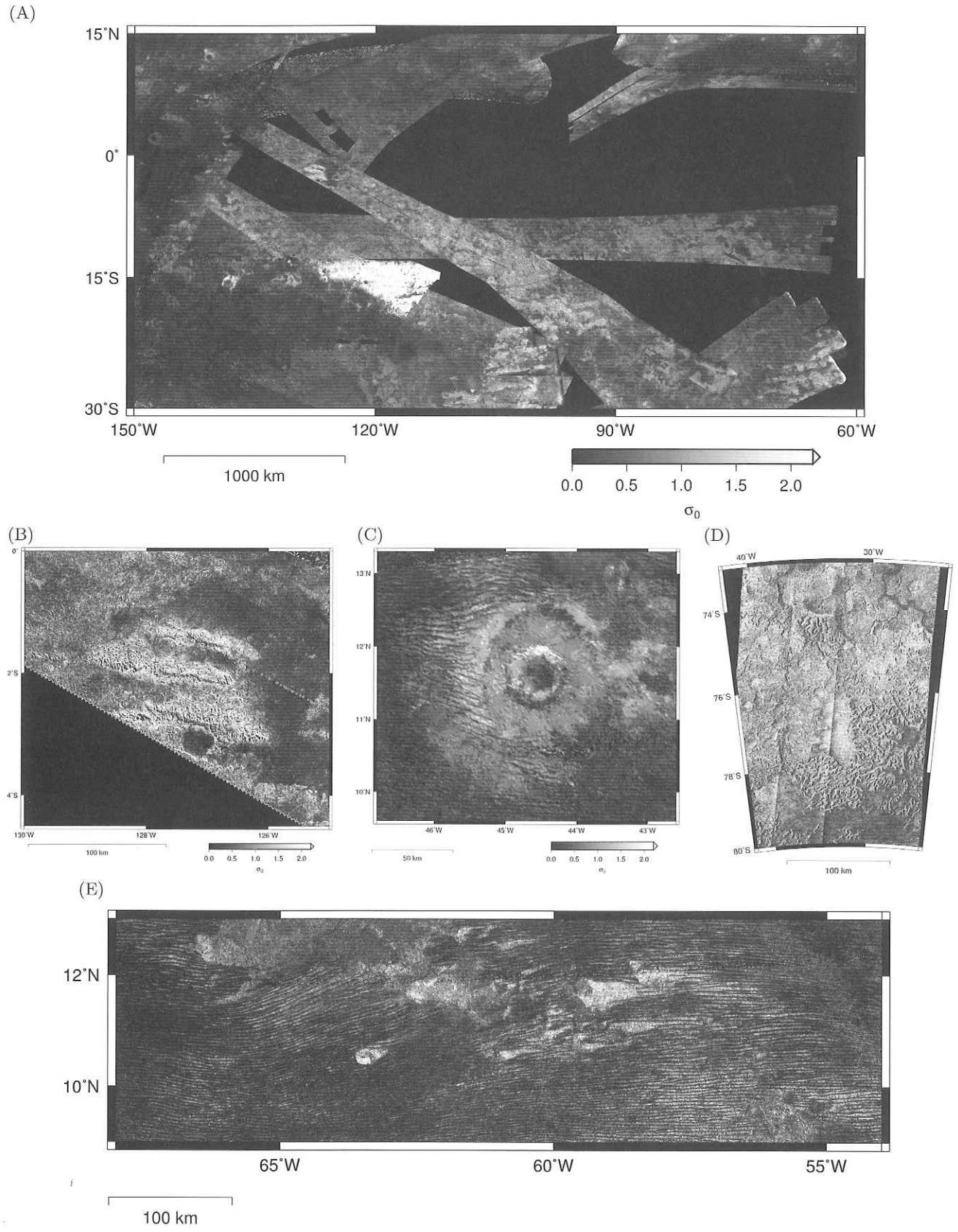

Figure 2.2 (A) The Xanadu province (mosaic of SAR images), (B) mountain ranges (T43; May 2008) (C) impact crater Momoy (T77; June 2011) (D) labyrinthic terrain (T39; December 2007) and (E) longitudinal dunes (T77; June 2011).

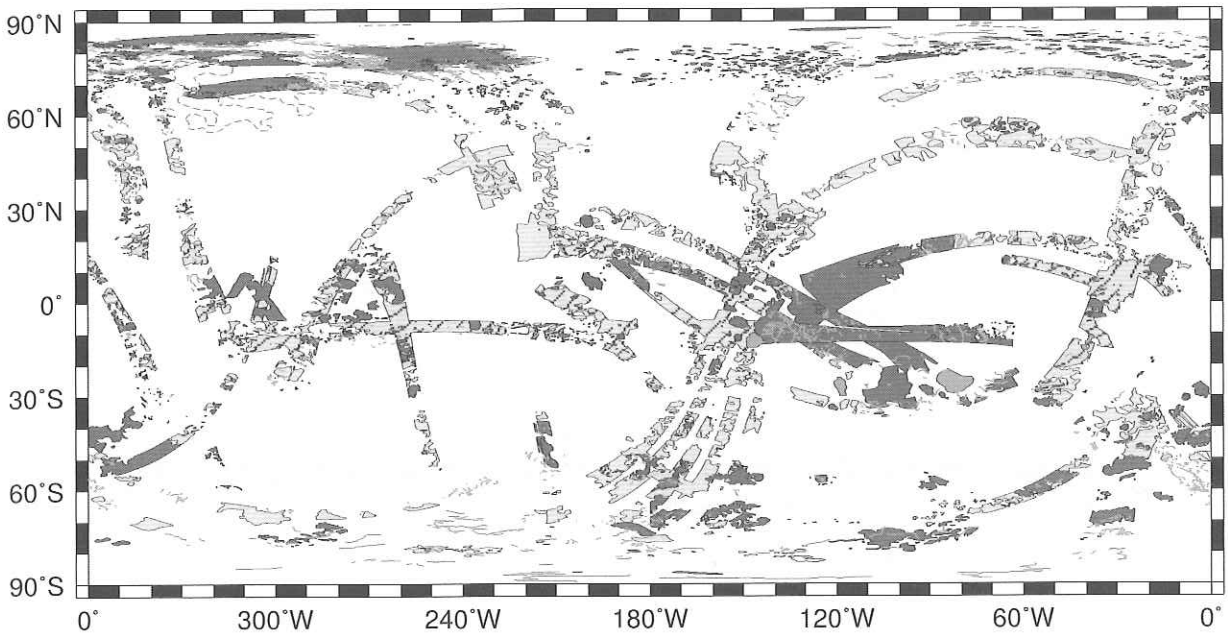

Geomorphic Units			
Plains	Hummocky Terrain	Labyrinthic Terrain	Dunes
Cryovolcanic Candidates	Impact Craters		Crateriform Structures
Seas/Lakes	Partially Filled Lakes		Empty Lakes
ISS Dark Areas	Fluvial Valleys		SAR Coverage

Figure 2.3 Geologic unit map, with classifications based on Lopes et al. (2010). (See color plate.)

by 1000 to 2000 m above their immediate surrounding terrain (Radebaugh et al., 2011).

Xanadu, an equatorial feature about 4500 km across, was first detected using the Hubble Space Telescope (Smith et al., 1996) and is the brightest and largest geologic feature on Titan's surface (Figure 2.2(A)). It is observed to have a high albedo at all wavelengths interrogated by *Cassini* (optical, infrared, and microwave). In fact, portions of Xanadu and the bright hummocky terrain are among the most radar-bright surfaces encountered in the solar system. Comparisons between active and passive microwave measurements of Xanadu have led Janssen et al. (2011) to conclude that the terrain must have an ordered, nonrandom structure in its surface or subsurface to explain its anomalously high backscatter and near-unity polarization ratio. The overall elevation of Xanadu is low compared with surrounding dune fields; however, the terrains that make up the Xanadu region are some of the most rugged and mountainous on Titan (Radebaugh et al., 2011).

Xanadu was initially thought to be distinct from the rest of Titan's surface due to its large size, near infrared brightness contrast, and distinctive microwave scattering properties (Janssen et al., 2009, 2011; Wye et al., 2007; Radebaugh et al., 2009). However, Lopes et al. (2010) argued that, geomorphologically, Xanadu is very similar to the terrains seen in the hummocky and mountainous terrain. They recognized, however, that at smaller scales, several other types of units are seen within Xanadu, including structures that may be flows (Wall et al., 2009), fluvial valleys, and crateriform structures (Wood et al., 2010; Radebaugh et al., 2009). Also, from VIMS spectra, there are differences between Xanadu and other hummocky and mountainous materials (Barnes et al., 2007). A detailed study of the Xanadu region, which further divides it into several units, is presented in Radebaugh et al. (2009). The hummocky and mountainous terrain unit, including Xanadu, is thought to be the oldest geologic unit exposed on Titan's surface (Lopes et al., 2010) (Figure 2.2(A)). It is extensive,

making up about 14 percent of the surface mapped to date. Brown et al. (2011) have recently suggested that the geomorphology of Xanadu is consistent with the site of an ancient impact, but the origin of Xanadu remains enigmatic.

Impact craters unit: Few impact craters have been unambiguously identified on Titan. These include the named craters Menrva, Sinlap, Ksa, Afekan, Selk, Hano, Soi, and Momoy. These craters and their associated ejecta blankets, where they are discernible, are mapped as the impact crater unit. However, there are numerous structures on Titan that may have been caused by impact. Radar-bright and near-IR-bright complete or incomplete circular features are seen throughout the surface, but these features are not sufficiently well defined to allow a confident interpretation of their origin. In some cases the circular outline is clear (for example, as shown in Figure 2.2(C)), but burial by surrounding material obscures possible ejecta blankets, making their origins uncertain. Wood et al. (2010) identified forty-four possible impact craters with a wide variety of morphologies and, since then, others have been recognized and mapped. Wood et al. (2010) assigned degrees of confidence to these craters; we refer to all but the most certain identifications as crateriform structures. Craters and crateriform structures are located mostly at low latitudes, with no confidently identified craters poleward of 60 degrees, possibly indicating that more resurfacing has occurred at higher latitudes. In terms of areal extent, craters and their ejecta deposits cover only about 1 percent of Titan's mapped surface, whereas crateriform structures cover around 0.2 percent. Stereo-based topography from RADAR images reveal a depth-diameter ratio for Titan's craters that is shallower than models predict (Kirk et al., 2011), possibly due to filling and relaxation of the depression subsequent to formation. Some craters exhibit flow features in their ejecta fields, as seen in the Selk crater (Soderblom et al., 2010) and a crater in a RADAR image from *Cassini* pass T77 (Kirk et al., 2011).

Dunes unit: Aeolian transportation and deposition is a major and widespread process on Titan. Features resembling both linear and crescentic dunes on Earth have been identified by SAR, covering regions hundreds, sometimes thousands, of kilometers in extent (Lorenz et al., 2006a; Radebaugh et al., 2010) (Figure 2.2(E)). Their presence indicates the production of a significant supply of easily mobilized sand-sized particles, winds capable of saltation, and conditions dry enough to permit sand transport near Titan's equatorial latitudes. Dune fields cover around 18 percent of Titan's mapped surface and are located mostly at low latitudes, within ~30 degrees of the equator (Radebaugh et al., 2008; Lopes et al., 2010). Dunes are dark to RADAR and ISS and correlate well with dark surface units identified by VIMS (see Surface Composition section). The dunes are thought to be made of organic particles (Soderblom et al., 2007), which may have originated as photochemical debris precipitated from the atmosphere, deposited, accreted (by an unknown process), and perhaps later eroded by fluvial processes (Atreya et al., 2006; Soderblom et al., 2007). Dunes have been observed within impact structures (Buratti et al., 2012). The mechanism for growing aerosols or grinding particles to sand-sized sediment that can saltate and form dunes on Titan remains uncertain. An example of the dune unit is shown in Figure 2.2(E).

Fluvial valleys unit: Many fluvial features are observed in SAR images, suggesting that they are widely distributed on Titan. In fact, it is likely that many more fluvial valleys and channels exist on Titan than those presently observed, but are too small for SAR data to resolve. Such small-scale fluvial features are visible in the *Huygens* descent images taken near the equator (Tomasko et al., 2005). Although approximately half of Titan's surface has currently been imaged at a resolution of a few hundred meters, some trends in the spatial distribution of the fluvial networks resolved by these images can tentatively be identified. Fluvial networks are widespread, occurring over nearly the full range of surveyed latitudes (Lorenz et al., 2008), and many are associated with polar lakes (Langhans et al., 2011; Burr et al., 2013; Figure 2.4).

Features commonly assumed to be fluvial in origin are visible as both radar-bright and radar-dark features with small width-to-length ratios that intersect to form networks (Elachi et al., 2005; Lorenz et al., 2008; Figure 2.5). Paired dark and light bands in some RADAR images (Lorenz et al., 2008; Burr et al., 2009) and a topographic map derived from stereo images near the *Huygens* landing site (Tomasko et al., 2005; Soderblom et al., 2007) demonstrate that at least some of the networks are valleys, rather than merely differences in surface composition or texture. The majority of the

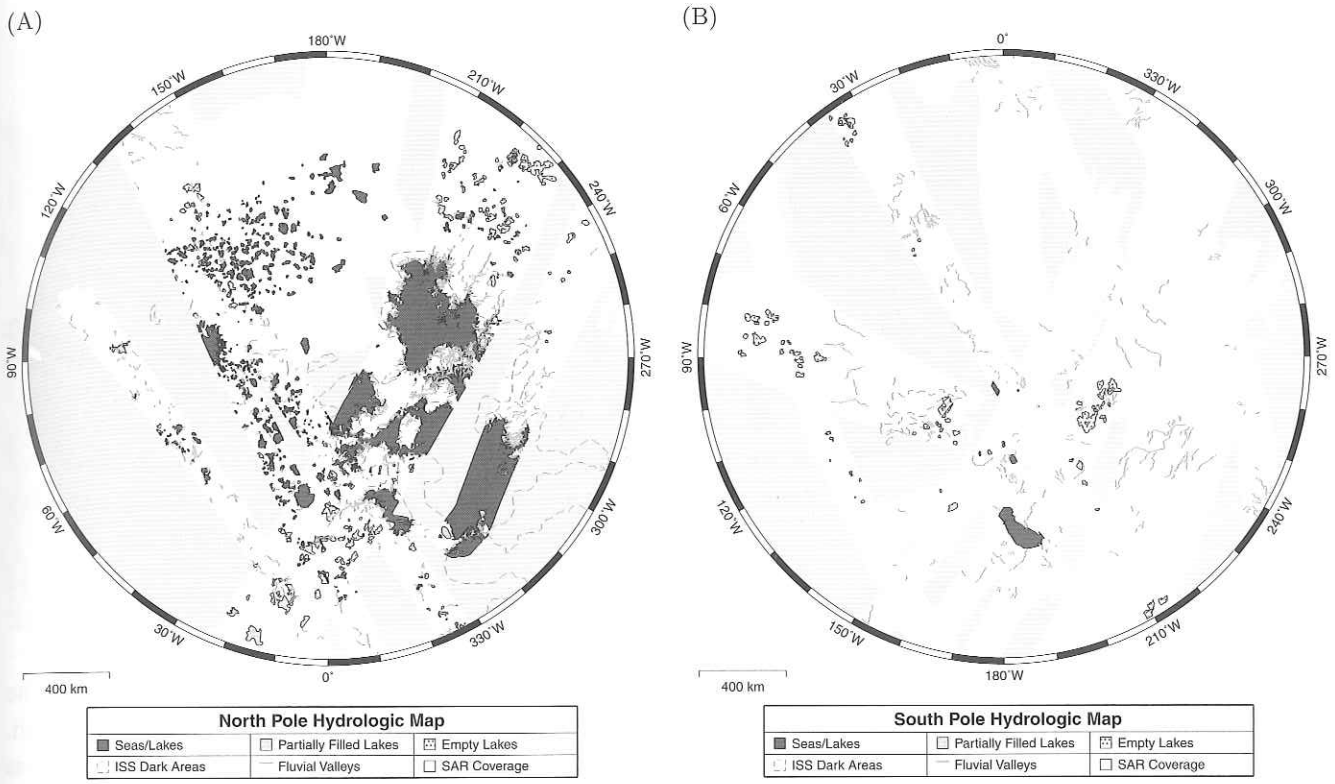

Figure 2.4 Distribution of hydrologic features on Titan poleward of 55°. The maps indicate filled lakes, partially filled lakes, empty lakes, and incised valleys in the north (A) and south (B). The widths of valleys have been exaggerated for visibility. (See color plate.)

observed features are tributary networks with locally consistent orientations, suggesting that they were created by flows that originated from distributed sources and merged as they traveled down the local topographic gradient. As discussed later, these characteristics are consistent with the interpretation that fluvial features were formed by methane precipitation, which recent observations suggest may be ongoing (Turtle et al., 2011a). In some cases, features widen in the inferred downstream direction, suggesting that valley width, and possibly depth, scale with flow discharge. Most features are many times longer than they are wide (Barnes et al., 2007), and appear to follow a single path rather than splitting into multiple threads. There are, however, a few examples of apparent distributary networks (Lorenz et al., 2008; Burr et al., 2013), suggesting that flows may have constructed depositional features at locations where there is a sudden reduction in sediment or solute transport capacity. A few areas where valleys appear to have disgorged have been mapped, such as Leilah Fluctus (Lopes et al., 2010) and Elivagar Flumina, which Lorenz et al. (2008) interpreted as alluvial due to its spatial proximity to fluvial valleys and its radar backscatter, which is similar to that of materials within fluvial valleys.

Fluvial features flow into some lakes at high latitudes (e.g., Figure 2.6) and through the hummocky, mountainous terrain at lower latitudes, possibly indicating orographic rainfall. Fluvial features, lakes, and dunes are thought to be the youngest morphologic units on Titan (Lopes et al., 2010). While the temporal relationship between fluvial features and dunes is not clear, at currently available resolution and coverage no fluvial features are observed to disrupt dune crestlines.

If the features described here are indeed fluvial valleys, they almost certainly contain channels – open conduits through which the flows pass – but it is difficult to conclusively identify channels. One possible channel on a valley floor is shown in Figure 2.5. Thus, there are currently no direct measurements of the cross-sectional or plan geometry of the channels except the upper bounds placed by the valleys within which they are presumed to reside.

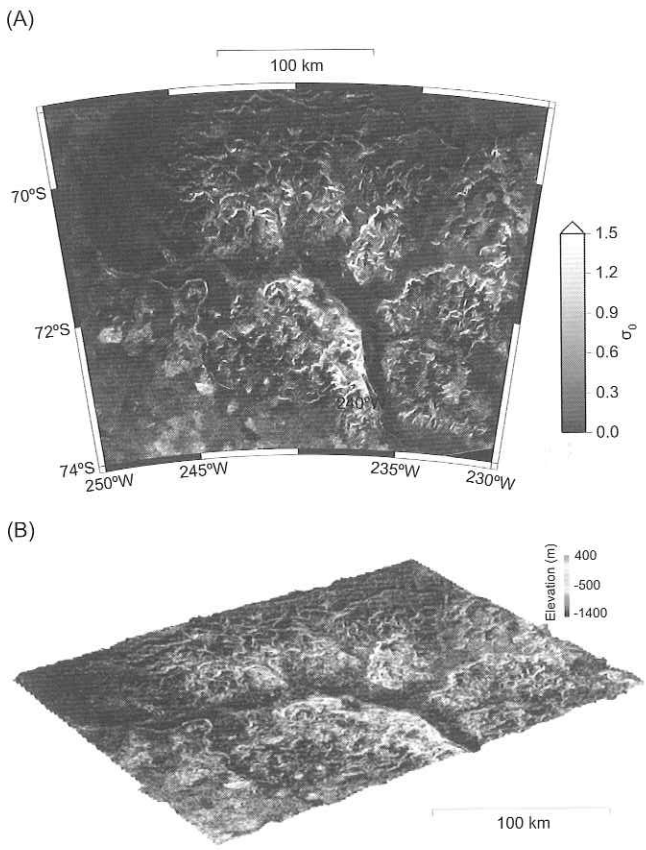

Figure 2.5 (A) Example of a fluvial network near the south pole, shown in a denoised SAR image. A possible channel appears at the floor of the broadly incised valley. (B) The image is draped over topography derived from a pair of SAR images obtained in June 2009 (T55 and T56). (See color plate.)

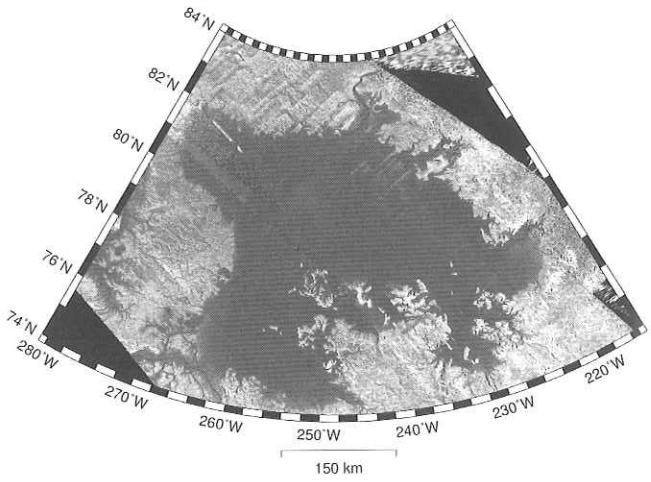

Figure 2.6 Mosaic of SAR images showing Ligeia Mare (T25, February 2007; T28, April 2007; T29, April 2007). The images have been colorized to emphasize the land/liquid contrast in backscatter value. (See color plate.)

The uncertainty regarding channel dimensions compounds the already difficult challenge of interpreting remotely sensed characteristics of fluvial features. The channel width may be sufficiently small relative to the valley width (and the pixel size of the sensor) that remote observations are dominated by characteristics of the valley surface, although the signature of the channel could still be detectable if it has a large amplitude and differs substantially from the surrounding landscape. A specific example of a remotely sensed signature without a clear interpretation is that some fluvial features appear darker than the surrounding terrain in RADAR images, whereas others appear brighter. It seems likely that the overall reflectance of the valleys is strongly influenced by the composition and roughness of the valley walls, although the reflectance characteristics of fluvially transported sediment could potentially have a significant influence (Le Gall et al., 2010), even if the channel width is a small fraction of the valley width. But the specific reason why the sign of the brightness difference between a valley and its surroundings varies among locations is not obvious. Even if it is difficult to reliably infer characteristics of channel beds from remote measurements, the observation of abundant, unconsolidated sediment on the surface at the *Huygens* probe landing site suggests that channels do not flow over a sheer bedrock surface in all locations.

Lakes units: Lake units have been subdivided into radar-dark lakes (interpreted as deep enough to absorb the incident microwave radiation), seas (large enough that they are designated maria by the International Astronomical Union), granular lakes (interpreted as shallow enough to see through with the RADAR or exposed saturated regolith), and empty lakes following Hayes et al. (2008) (see Figure 2.11). Empty lakes are thought to be lakes that have drained or evaporated. They occupy depressions that are not currently filled with dark materials, although they can exhibit different radar properties from their surrounds. Dark lakes and seas are characterized by extremely low (often below the instrument noise floor) radar returns, indicative of an unusually smooth or absorptive material at 2.2 cm wavelength, and are interpreted to be standing bodies of liquids (Figure 2.6). Supporting this hypothesis is the identification by VIMS of liquid ethane in Ontario

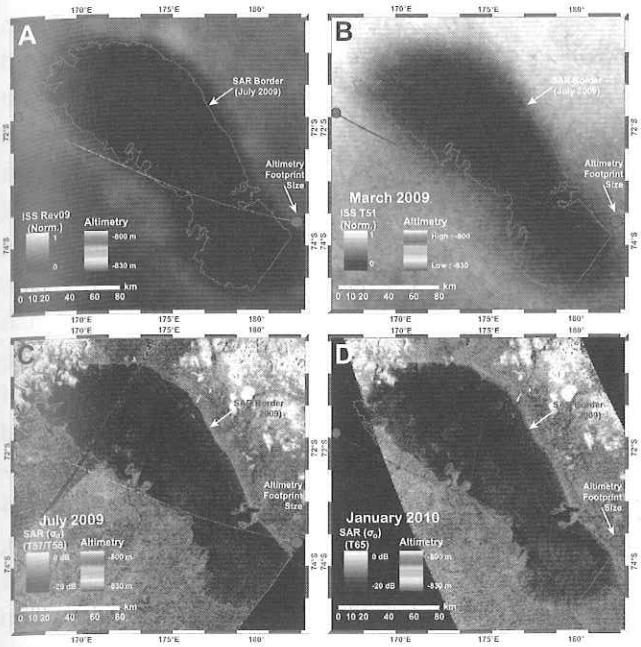

Figure 2.7 Tracking changes of Ontario Lacus. The lake border from the 2009 SAR observation is shown in blue in all panels. December 2008 (T49) altimetry data is overlaid. Heights are calculated from echo center-of-mass and referenced to Titan's geoid as presented in Iess et al. (2010). Altimetry footprint size is shown using blue circles; (A) ISS image obtained in June 2005 (Rev09). (B) ISS image obtained in March 2009 (T51). (C) SAR image obtained in June and July 2009 (T57/T58). (D) SAR image obtained in January 2010 (T65). (See color plate.)

Lacus (Brown et al., 2008), a feature at high southern latitudes that ISS images first identified as a lake. Filled lakes are mostly found at high northern latitudes, with only a few at high southern latitudes (Aharonson et al., 2009). In terms of areal coverage, lakes cover only about 1.5 percent of Titan's mapped surface.

Lakes likely form due to rainfall (Mitri et al., 2007), but the location and extent of lakes may be affected considerably by evaporation, surface runoff, and subsurface flow (Hayes et al., 2008). Many, but not all, lakes occupy steep-sided depressions that appear to exist primarily in the same high-latitude regions, implying a causal relationship.

Liquid hydrocarbons such as methane and ethane absorb strongly within the methane windows accessible to VIMS, and appear nearly black to VIMS when the liquid path length is deeper than a few centimeters (Clark et al., 2010). One south polar lake, Ontario Lacus (Figure 2.7), displays a narrow absorption within the 2.0 μm window, which has been attributed to liquid ethane (Brown et al., 2008). Specular reflections from the north polar lakes Kraken Mare and Jingpo Lacus, measured by VIMS in the 5 μm window (Stephan et al., 2010), and the south polar lake Ontario Lacus, measured by RADAR (Wye et al., 2009), were consistent with a lack of wave activity, indicating that these features are much calmer than their terrestrial counterparts (Stephan et al., 2010; Barnes et al., 2011b).

Cryovolcanic candidates unit: Cryovolcanism, the presence of which has yet to be unequivocally demonstrated, may serve to resupply Titan's atmosphere with methane, which is destroyed via photolysis in the upper atmosphere. SAR observations have revealed several lobate, flowlike features and constructs that have been interpreted as potentially cryovolcanic in origin (Elachi et al., 2005; Lopes et al., 2007; Wall et al., 2009; Soderblom et al., 2009). VIMS data have also identified some features that were thought to be cryovolcanic in origin (Sotin et al., 2005; Barnes et al., 2006; Nelson et al., 2009a,b). However, as more data were acquired, particularly overlapping SAR coverage from which stereotopography could be derived, several units initially interpreted as cryovolcanic, such as Ganesa Macula and Tortola Facula, were reassessed (Lopes et al., 2010) leading Moore and Pappalardo (2011) to argue that there may not be cryovolcanic units on Titan at all. The units mapped herein consist of candidate cryovolcanic features as discussed by Lopes et al. (2011). Candidate cryovolcanic features are not ubiquitous on Titan, and cover only about 0.6 percent of Titan's mapped surface. They show a somewhat narrow longitudinal distribution, between 30°W and 120°W. However, as discussed below, only two regions remain as strong candidates for a cryovolcanic origin, Sotra Facula (Figure 2.8) and the flows within Hotei Regio.

Labyrinthic terrains unit: This unit was identified by Malaska et al. (2010) as a probable end-member of the different types of channel and valley network morphologies identified on Titan (Figure 2.2(D)). There are few areas of this type of terrain exposed, mostly at high latitudes, making up only about 0.19 percent of Titan's mapped surface.

Undifferentiated plains unit: There are vast expanses of plains, mostly at mid-latitudes, that appear relatively homogeneous and radar-dark, and are classified

Figure 2.8 A RADAR image of Sotra Facula, draped over a DEM generated from an image pair obtained in February and April 2007 (T25 and T28). VIMS data in color shows the dune fields in blue and the candidate cryovolcanic features in shades of green and brown (NASA PIA13695). The mountain is ~1.5 km high, and vertical exaggeration is 10:1. (See color plate.)

as plains because they are areally extensive, relatively featureless, and generally appear to be of low relief (e.g., Elachi et al., 2005; Stofan et al., 2006). Plains units tend to have gradational boundaries, and occur in patches that are generally hundreds of kilometers in extent. The gradational boundaries make it difficult to distinguish possible different types of plains within this unit. The units may be sedimentary in origin, resulting from fluvial or lacustrine deposition or the accumulation of photolysis products created in the upper atmosphere. The plains may also be cryovolcanic, but their relatively featureless nature and gradational boundaries in SAR dara hinder interpretation, and the VIMS data suggest they are compositionally diverse. They cover around 14 percent of Titan's mapped surface and are mostly located at mid-latitudes.

Mottled plains unit: The mottled plains are irregularly shaped terrains having dominantly intermediate backscatter and relatively small topographic variations. These terrains contain patches of radar-dark and -bright materials. They sometimes flank hummocky and mountainous terrain. Patches of mottled plains extend from tens to hundreds of kilometers. Stofan et al. (2006) interpreted the radar brightness variations in these units to be likely dominated by roughness variations produced by fracturing and erosion of Titan's icy surface, along with some contribution from volume scattering and compositional variations. However, so far the mottled terrains have not been mapped on a global scale, mostly because it has not been possible to determine if different exposures of mottled terrains on different parts of the surface have the same characteristics and the same possible origin. Mottled terrains may be erosional and a mix of several other units; for example, some may be undifferentiated plains covered over in small areas by isolated dunes.

2.3 Surface composition

Titan's surface is largely obscured in the visible and near-infrared by atmospheric absorption and scattering, except in several methane windows where compositional units are mapped. Based on its 938-nm albedo, the surface of Titan can be divided into two units: a "bright" unit that corresponds primarily to Xanadu and mid-latitude terrain, and a "dark" unit, which is largely confined to the equatorial regions (Porco et al., 2005). Prior to *Cassini*, Earth-based observations of Titan in the near infrared distinguished these two units as an albedo contrast between the leading (Xanadu) and trailing hemispheres, and also suggested that the disk-integrated spectrum of Titan is consistent with surface exposures of nearly pure water ice, possibly contaminated with small amounts of precipitated hydrocarbons (Griffith et al., 2003; Coustenis et al., 2006). However, these observations could not rule out the presence of other ices (e.g., CO_2, ammonia hydrate) or liquid hydrocarbons on the surface.

The first VIMS spectra of Titan showed the dark unit to be broadly consistent with contaminated water ice, but only if the reversal in spectral slope at the poorly understood 2.8-μm window is ignored (McCord et al., 2006) (Figure 2.9). Although the dark equatorial unit appears to be compositionally uniform and consistent with "dirty water ice," McCord et al. (2006) also found that the bright unit exhibits greater spectral diversity, but could not be matched with pure forms of predicted materials, including water ice, tholin, pure hydrocarbons, and ammonia. Dividing the dark terrain into "brown" and "blue" subunits based on their spectral slopes between 1.3 and 2.0 μm, Soderblom et al. (2007) found the reflectance spectrum of the dark blue unit to be consistent with greater enrichment in water ice relative to the dark brown unit. Comparisons with radar data revealed the dark brown unit to be strongly

correlated with the equatorial dunes, whereas the dark blue unit occurs primarily on the dune-free sides of topographic obstructions within the fields. This observation led Soderblom et al. (2007) to interpret the dark blue unit as water-ice-rich "bedrock" underlying both the dark brown dunes unit and each of the bright subunits. Because the dark brown unit is slightly less absorbing in the 1.6 and 2.0 μm water bands than the dark blue unit, these authors suggested that the dune particles could be composed primarily of hydrocarbons and nitriles expected to precipitate from the atmosphere. They further suggested that the bright subunits, which are much more reflective at 1.6 and 2.0 μm, could be composed of fine tholin dust precipitated from the atmosphere, but did not interpret the spectral variations among these subunits.

Barnes et al. (2008) investigated the composition of the dunes, as well as the inter-dune material, using VIMS reflectance spectra with high spatial resolution of order a few km/pixel. These authors suggested the dunes are depleted in water ice relative to the average Titan surface, based on their low reflectance at 1.1 and 1.3 μm and their positive 2.8/2.7 μm reflectance ratio. However, atmospheric effects have so far prevented quantitative estimates of water ice concentrations within geologic units on Titan's surface, and it should be noted that water ice cannot yet be ruled out as a constituent of the dunes based on VIMS spectra alone. On the other hand, the low radar dielectric constant of ~1.6 estimated for those regions supports that the dune materials are depleted in water ice (Janssen et al., 2009; Le Gall et al., 2011). This value would be consistent only with water ice with unreasonably high porosities for the dunes. The question of the abundance of water ice on the surfaces and interiors of dune particles remains open.

Titan's bright terrain can be separated into several subunits based primarily on variations in reflectance among the 1.3, 1.6, 2.0, 2.8, and 5.0 μm windows, as well as the 2.8/2.7 μm ratio. Standing out among the bright subunits are Tui Regio and Hotei Regio, which are prototypes of the compositional endmember classified as "5-μm-bright" (Barnes et al., 2005; McCord et al., 2006). The overall spectral shape of this endmember and its strongly positive 2.8/2.7 μm ratio are consistent with the reflectance spectrum of fine-grained CO_2 frost (McCord et al., 2008), which is a photochemical product predicted to precipitate to the surface (Atreya et al., 2006; Coustenis et al., 1995). However, correction for atmospheric effects suggests a lower 2.8/2.7 μm ratio, which is not consistent with

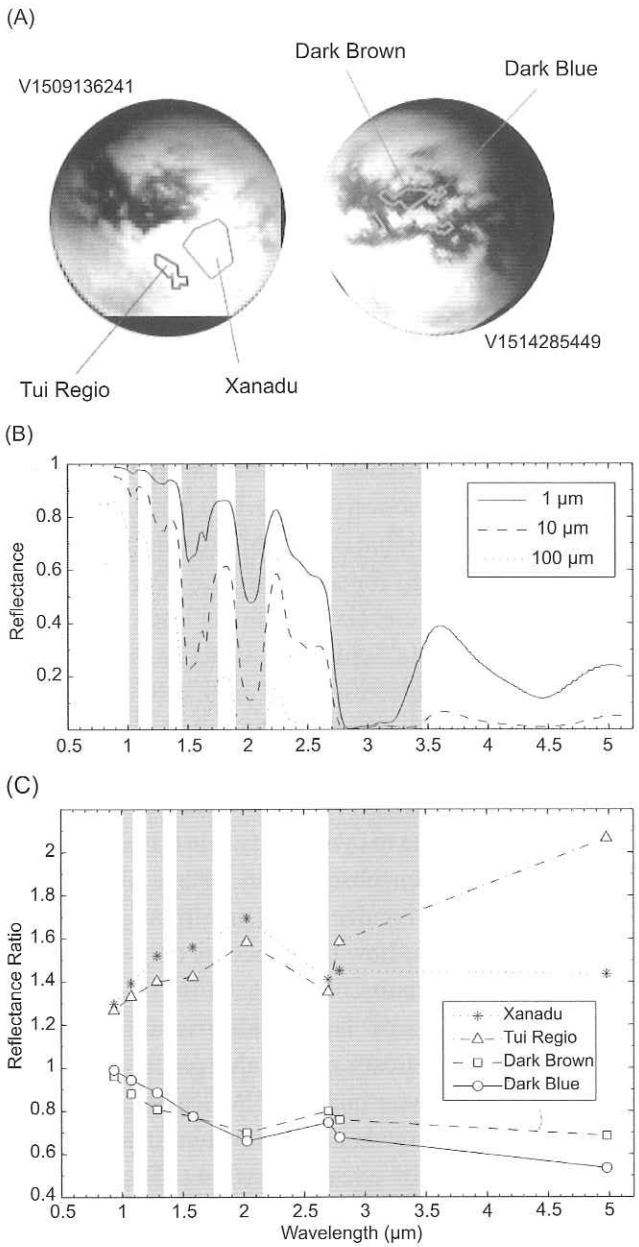

Figure 2.9 (A) Regions of interest selected shown on a VIMS image mosaic adapted from Barnes et al. (2009b). (B) Model spectra for granular water ice deposits, calculated using the albedo model of Wiscombe and Warren (1980), and optical constants of Warren and Brandt (2008), for three values of the mode grain radius. (C) VIMS averaged spectra for representative compositional classes on the surface. The reflectance ratio is the calibrated reflectance (I/F) normalized by the full disk average, consistent with the results of McCord et al. (2006, 2008).

pure CO_2, though mixtures with water ice are not ruled out by the VIMS data (Clark et al., 2010). Barnes et al. (2011a) found that radar-bright depressions found in the north polar region, interpreted as empty lakes by Hayes et al. (2008), are also members of the "5-μm-bright" spectral end-member and interpreted them as potential evaporate deposits. Barnes et al. (2008) observed that the inter-dune material is variable in composition, but is composed primarily of the bright materials, including the 5-μm-bright unit exemplified by Tui Regio and Hotei Regio.

In the near-infrared, the 5 μm methane window is the broadest and least affected by aerosol scattering, which has allowed the discovery of several narrow absorptions due to vibrational bands of surface molecules. McCord et al. (2008) found a narrow 4.92-μm absorption that is strongly correlated with Tui Regio and Hotei Regio ("5-μm-bright" unit), but were unable to identify the absorbing species. Clark et al. (2010) used the same technique to find hydrocarbons and nitriles, such as benzene, condensed predominantly within the dark surface units, and also presented evidence that the 4.92-μm absorption is due to cyanoacetylene (HC_3N). These molecules have been observed in Titan's atmosphere and are expected to condense and precipitate to the surface, but it is unclear how they become concentrated in particular geologic units.

The composition of Titan's lakes is an intriguing question, with implications for the global hydrocarbon cycle and reservoir budget. VIMS spectra acquired over Ontario Lacus when it was illuminated in late summer indicate that ethane is present (Brown et al., 2008), likely in liquid solution with methane, nitrogen, and other low-molecular-mass hydrocarbons that are difficult to detect through the atmosphere. Recent VIMS observations of northern lakes also show evidence for ethane (Soderblom et al., 2012). This must be reconciled with the expected large atmospheric fluxes of the more volatile species methane, predicted in GCMs (Schneider et al., 2012; Mitchell, 2008) and observed to have been lost from lake level changes in the south (Hayes et al., 2011a; Turtle et al., 2009, 2011b). Becuase methane is positively buoyant in ethane, if unmixed, a compositionally stratified lake would likely only increase in ethane abundance with depth. Stronger compositional constraints of the lakes await future measurements, from orbit or by a lake lander.

2.4 Aeolian processes

The first identification of dunes resulted from the third *Cassini* fly-by of Titan (T3) in February 2005, when SAR images revealed linear forms interpreted to be longitudinal dunes created in a variable, likely bimodal, wind regime (Elachi et al., 2006). Dunes are most distinctly mapped in SAR images, as their typically radar-dark returns contrast with the radar-brighter inter-dunes (depending on illumination geometry, the contrast is occasionally reversed; see Figure 2.2(E)). Indeed, to radar, the dunes are the least reflective (and most emissive) of Titan's solid surface materials. It is noteworthy earlier ISS images acquired in the first two Titan passes were interpreted to contain streaks, with morphology indicating west-to-east transport on the basis of their abrupt westerly and diffuse easterly boundaries (Porco et al., 2005).

The prevalence of dunes on the surface attests to the production, transport, and organization in patterns of sand particles. The dunes are among the youngest surface features, as they are not seen to be superposed by other features such as fluvial valleys or craters. The sand seas in the Namib and Sahara deserts on Earth are most analogous to the linear forms and scale of dunes on Titan.

Surveys of dune distribution and orientation in the SAR data set reveal patterns. Dunes are largely restricted to a latitude band within 30° of the equator (Figure 2.3), and their longitudinal axis is predominantly oriented in the east-west direction (Lorenz and Radebaugh, 2009). Some deflection from this direction is seen, but the deviation angle is generally 10° or smaller and typically associated with deflection around topographic obstacles (Barnes et al., 2008). The global areal coverage by dunes is 12.5 percent, and the zonal average fraction can exceed one half near the equator (Le Gall et al., 2011). If composed of organics, the inferred heights and vastness of the dunes render them the largest reservoir of hydrocarbon on Titan estimated at roughly 250,000 km^3 (Le Gall et al., 2011) assuming 100 m high dunes (although an uncertainty of a factor of a few remains). If the dune material is dominantly hydrocarbon, this largest identifiable reservoir may be compared to model-based predictions of hydrocarbon production by photolysis over the age of the solar system (Lorenz, 1996). By some estimates the

production, if continuous, still exceeds the observed volume, suggesting either the models are overestimating the production rate/duration, additional unseen reservoirs are present, or a sink is actively depleting the material (Lorenz et al., 2008a).

Dunes form by saltating particles, the optimum size for which on Titan is ~0.18 to 0.25 mm (Lorenz et al., 2006b, and references therein), balancing the wind's lifting capacity with the tendency of small grains to clump. However, considerable uncertainty exists because cohesive forces between hydrocarbon grains at Titan conditions are not well measured. The particles may result from either breakup/erosion of larger particles or merger/growth of smaller particles. Lacking knowledge of the particle size distribution and compositional heterogeneity, both options remain viable.

The largest sand sea on Titan is the Belet sand sea (220–300°W, 20°S–20°N). The sediment supply in this region grades from the central portion to higher latitudes in Belet. Near the center, dunes are long and closely spaced and the interdunes appear sand covered, based on SAR images. Near the edge the dunes are shorter, more widely spaced, and the interdunes appear sand-free (Radebaugh et al., 2011). The smaller Fensal sand sea (30–90°W, 5°S–20°N) exhibits sparser dunes, more exposed interdunes, and hence is interpreted to have a thinner sand cover relative to Belet. The trend of lower sediment cover is consistent across RADAR, ISS, and VIMS images (Radebaugh et al., 2011). In this region, radar altimetry profiles suggest the dunes are deposited on a relatively smooth substrate with a variation in topography of ~100 m over ~475 km (Le Gall et al., 2011). The exposed interdunes expanses have been suggested to imply recent activity (Le Gall et al., 2011), sweeping surfaces clean of presumed airfall hydrocarbon particles. Shangri-La (150–200°W, 20°S–20°N) again exhibits a thicker sediment, with dunes occasionally covering topographic obstacles, such as the putative impact crater Guabanito (Wood et al., 2010; Radebaugh et al., 2010). RADAR data from multiple locations show the inter-dune fraction increases northward (Le Gall et al., 2011), interpreted to indicate a reduced sediment availability.

Geometric properties of dunes have been measured with several techniques. SAR images, particularly when denoised may be used to estimate dune wavelengths

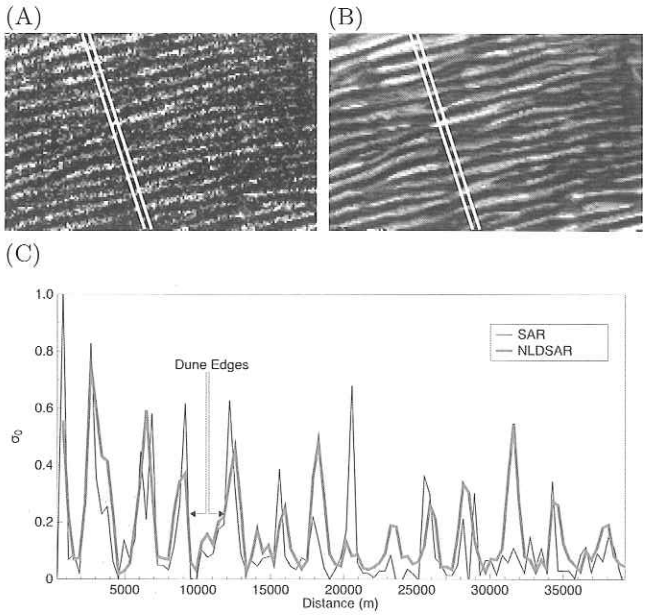

Figure 2.10 (A) Comparison between SAR image and (B) its denoised counterpart of longitudinal dunes (T17; September 2006). (C) Cross sections of back-scatter extracted from the SAR and denoised images, showing the denoised data improves measurement of the peridiodicity while conserving the dune's edges. Spectral decomposition reveals the dominant dune's wavelength of ~3200 m.

(Figure 2.10), which are often constant over large areas. For study areas in Belet and in Shangri-La, Neish et al. (2010) found robust dune heights of 45 to 180 m, and dune spacing of 2.3 to 3.3 km by employing radarclinometry validated against comparable observations of the Namibian dunes. These heights are in agreement with 150 m dunes, again from radarclinometry in Belet (Lorenz et al., 2006a), and are somewhat higher than those seen by VIMS photoclinometry further north (Barnes et al., 2008). Dune lengths in Belet average ~38 km (Radebaugh et al., 2008), and although dunes of comparable size appear elsewhere on Titan, characteristic lengths vary.

As described previously, VIMS spectra indicate dunes are depleted in water-ice relative to the "dark blue" unit often observed adjacent to and in between dunes (Barnes et al., 2008). Reflectance spectra may result from microns-thick coatings, so a water-ice-rich core in the sub-millimeter dune particles cannot be ruled out using VIMS data alone. However, the radiometric properties of dune areas are consistent with

porous organics, but not pure water ice, with an effective dielectric constant of ~1.6 based on their passive polarization ratio (Paganelli et al., 2007; Janssen et al., 2009).

The dunes on Titan are generally (though not universally) observed to have long, linear, parallel crests, and are hence classified as linear dunes. On Earth, such dunes are generally associated with either a setting where the dominant wind alternates between two directions, or by local stabilization of the sediment. In analogy with admittedly smaller and more variable dunes in the Qaidam Basin, China, Rubin and Hesp (2009) suggest Titan's linear dunes form by stabilization of initially loose sediment. The dune form then acts as a topographic shelter, promoting deposition downwind. The stabilization mechanism, if correct, indicates the sediments are cohesive on Titan. However, the agent responsible for the grains sticking together, whether mechanical or by surface wetness remains unclear. At the edges of dune fields, crescentic crestlines are observed and interpreted as Barchans dunes, forming as a result of reduced sediment availability (Radebaugh et al., 2010).

Various mechanisms and associated wind regimes have been proposed to generate Titan's dunes. Dune crests are observed to divert around topography and abruptly end on the western side of obstacles, leading Lorenz and Radebaugh (2009) to suggest a west-to-east elongation direction. Like Earth's trade winds, Titan's equatorial winds are deflected toward the west by Coriolis forces, so an additional dynamical explanation, such as a cross equatorial flow, is required. Although agreement exists that zonal winds play a role, differences among models are present. Tokano (2008) finds obtuse bimodal winds in global circulation models with a tidal north-south component exceeding the zonal component. Lorenz et al. (2006a) argue for an influence of tidal winds to explain their longitudinal rather than transverse nature, as well as the misalignment of the dunes with the zonal direction. Radebaugh et al. (2008) appeal to a minor contribution of nonzonal winds to account for the dominance of east-west orientation, but quantitative limits are difficult to provide. Tokano (2010) suggests that seasonally reversing winds blow nearly perpendicular to dune crests, which are elongated eastward by occasional fast westerlies that occur during the equinox. Regardless of the wind regime responsible for their formation, the size scale and well-organized nature of the dunes suggest reorientation timescales of hundreds of kyr to 1 Myr (Werner and Kocurek, 1997; Hayes and Ewing, 2011). This implies that if the dunes are created by a bimodal wind, the duty cycle of wind variations need not be seasonal, and can in fact range up to these long timescales (Hayes and Ewing, 2011), and may be associated with orbitally driven insolation changes such as those suggested by Aharonson et al. (2009).

2.5 Lacustrine processes

Titan is the only extraterrestrial body currently known to support standing bodies of liquid on its surface and, along with Earth and Mars, is one of only three places in the solar system that we know to possess or have possessed an active hydrologic cycle. Lacustrine processes are an integral part of Titan's hydrologic system, providing both a source and sink for methane, ethane, and even higher-order hydrocarbons and nitriles. Liquid hydrocarbon lakes and seas were originally proposed as a source/sink for photolytic processes (Sagan and Dermott, 1982; Lunine et al., 1983; Yung et al., 1984) in response to the detection of methane in Titan's upper atmosphere (Kuiper, 1944; Hanel et al., 1981) and models of surface conditions derived from *Voyager's* radio occultation experiments (Lindal et al., 1983). Prior to *Cassini*, Earth-based observations using the Hubble Space Telescope (Smith et al., 1996) and the Arecibo radar (Campbell et al., 2003) searched for evidence of equatorial surface liquids. Although Campbell et al. (2003) did observe specular reflections using Arecibo's 12.6 cm radar, subsequent observations and comparisons with *Cassini* images (Black et al., 2011) suggest that these areas did not contain standing bodies of liquid. Although ephemeral lakes may have been present, the long wavelength of the Arecibo radar could have produced specular reflections from nonliquid surfaces and the detection of lakes remained ambiguous at best until *Cassini's* arrival.

The first direct evidence for lacustrine features on Titan was offered by ISS observations of Titan's south pole obtained in July 2004 (Rev00) and June 2005 (Rev09), which revealed more than 50 dark features poleward of 70°S (Porco et al., 2005; Turtle et al., 2009). However, the first high-resolution (~300 m) images of the lakes were not obtained until July 2006 (T16),

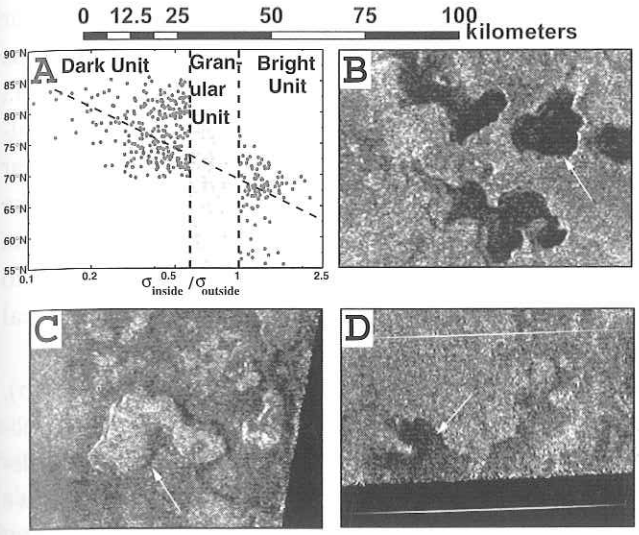

Figure 2.11 Lacustrine mapping units as defined by Hayes et al. (2008): (A) ratio between mean incidence-angle-corrected off-axis radar backscatter within and immediately surrounding feature, (B) filled lakes (dark unit), (C) empty lakes (bright unit), (D) partially filled lakes (granular unit).

when the RADAR detected more than 75 low backscatter features with distinctly lacustrine morphologies in the north (Stofan et al., 2007). Subsequent observations have revealed more than 650 lacustrine features scattered throughout Titan's polar regions, dominantly in the north (Hayes et al., 2008). To date, all three of *Cassini's* imaging instruments (ISS, RADAR, and VIMS) have observed these features and found that they have similar expression and are consistent with liquid-hydrocarbon-filled depressions (Hayes et al., 2008; Turtle et al., 2009; Sotin et al., 2011).

In mapping the lakes, Hayes et al. (2008) separated lacustrine features into three radiometrically distinct classifications: dark lakes, granular lakes, and bright lakes (Figure 2.11). All three classifications were defined based on the relative radar backscatter between the lake features and their immediate surroundings. Dark lakes, which are interpreted as liquid-filled basins, have returns that are near or below the *Cassini* RADAR's noise floor, consistent with a smooth surface at the scale of 2 cm. Bright lakes are interpreted as previously filled lake beds and have returns that are brighter than their surroundings at both nadir and off-nadir incidence angles. These empty lakes are found in nearby regions and have plan-view shapes that are similar in size and complexity to their filled counterparts. Granular lakes, which are interpreted as partially filled, have microwave scattering properties consistent with radiation either penetrating a liquid layer and interacting with the lake floor or, for the brighter examples, potentially interacting with saturated as opposed to dry regolith (Paillou et al., 2008a; Hayes et al., 2008, 2011a). In some cases, dark and granular lakes are found nested within larger depressions, the unfilled parts of which are consistent with bright lakes. The assignments are not always unique, with some ambiguity among the classes. Here the lakes are referred to by their interpreted filling state, as opposed to their restricted RADAR appearance.

Filled lakes account for 84 percent of all lake units mapped by Hayes et al. (2008) and have a log-normal surface area distribution with a median area of $\sim 77 \pm 20\ km^2$. Features with areas in excess of $10^4\ km^2$ represent 73 percent of the total lake area. The three largest lakes, namely Ligeia Mare, Kraken Mare, and Punga Mare, are similar in size to the Great Lakes of the midwestern United States. Although they are not apparent in the incomplete SAR coverage, VIMS and ISS observations suggest that Kraken and Ligeia Maria could be interconnected (Turtle et al., 2009; Sotin et al., 2011).

Partially filled lakes are not found poleward of 77° and represent 6 percent of lacustrine features by area (Hayes et al., 2008). The latitudinal emergence of partially filled lakes coincides with that of empty lake features, suggesting an evolutionary relationship. VIMS observations of the north polar region find that the majority of granular lakes observed by RADAR are indistinguishable from dark lakes (Sotin et al., 2011). If the granular lakes were filled with a shallow layer of liquid, VIMS would not be able to distinguish them from the deeper lakes that are also opaque to the RADAR. However, Barnes et al. (2011a) note that there are a few granular lakes that are not dark when observed at 5 μm. These features may represent areas of saturated regolith that would appear dark to RADAR, but could be indistinguishable from surrounding terrain as viewed by VIMS.

The depths of empty lake basins have been measured using altimetry, SAR-Topo, and RADAR stereogrammetry. Empty lakes are typically 150 to 300 m deep basins and represent 10 percent of all lake features by

area (Hayes et al., 2008). Similar to filled and partially filled lakes, the empty lakes have a log-normal area distribution, although the median area is slightly larger at 341 ± 100 km^2 (Hayes et al., 2008). In May 2007 (T30) RADAR acquired data from two empty lakes while in altimetry mode (Elachi et al., 1991), obtaining both topographic information and the microwave reflectivity of the lakebeds at nadir incidence. The results showed that the two empty lakes were brighter than their surroundings at both off-axis and nadir geometries, suggesting that they are compositionally and/or structurally distinct from surrounding terrain (Hayes et al., 2008). If the empty lakebeds simply had a rougher surface texture, they would have been significantly less reflective at nadir incidence. Recent observations made by VIMS show that the empty lakes are also bright at 5 μm, which Barnes et al. (2011a) argue is consistent with evaporite deposits.

The formation of the depressions that make up the empty lakes is not well understood. Three of the models that have been proposed include impact craters (Stofan et al., 2007), volcanic calderas (Wood et al., 2007), and karstic dissolution (Mitchell, 2008). The irregular shape of many lake features, nonstochastic size distribution, and concentration in polar regions argues against the impact and volcanic mechanisms as responsible for the majority of observed depressions. Their geographic association with, and geometric similarity to, filled lakes support a limnogenic origin. The karstic dissolution model requires a material that is soluble in liquid hydrocarbon to reside in abundance in the upper crust. Materials that have been suggested include acetylene, propyne, and/or clathrate (methane or carbon dioxide) (Mitchell et al., 2007). Water ice is not soluble in liquid hydrocarbon (Lorenz and Lunine, 1996). Karstic dissolution also implies subsurface interconnectivity and transport, as the dissolved material must be transported away in order to accommodate the resulting depressions. Some lakes are observed to have elevated rims, which are difficult to explain with purely karstic processes (Hayes et al., 2008; Mitchell, 2008).

Lacustrine features are confined to latitudes poleward of 55°, where around 60 percent of the surface has been observed by RADAR in both the north and south polar regions. Global SAR coverage (as of June 2011) encompasses 51 percent of the surface, 1.2 percent of which is covered with filled lakes. VIMS and ISS have obtained almost complete global coverage of the polar regions, although the reduced resolution (few to tens of kilometers) inhibits detailed mapping (Turtle et al., 2009; Sotin et al., 2011). Figure 2.4 shows the distribution of lacustrine features in the north and south polar regions; Table 2.1 lists the coverage statistics by lake type. In the south, lakes are about 26 times sparser than in the north and the largest lacustrine feature, Ontario Lacus, accounts for 95 percent of the lacustrine areal coverage observed by RADAR.

At the resolution of the *Cassini* SAR (~300 m), Titan's lakes express a range of morphologic characteristics. They are found both connected to and independent of regional and local drainage networks, have shoreline transitions varying from sharp to diffuse, include a variety of plan-form shapes ranging from near-circular to highly irregular, and have surface areas that span from the limits of detection of ~1 km^2 to more than 10^5 km^2 (Hayes et al., 2008). Isolated lakes imply either a direct link to the atmosphere or a deep drainage network, similar to seepage lakes found on Earth. Lakes with associated channel networks imply that they are dominated by surface runoff, similar to terrestrial drainage lakes. Both isolated and channel-fed morphologies are also found among the empty lakes. Other features, such as the shorelines of Kraken, Ligeia, and Pungea Maria and Ontario Lacus, have morphologies consistent with drowned topography (Stofan et al., 2008; Wall et al., 2010). Drowned river valleys found at the terminus of channels entering the seas imply a rising base level of the liquid flooding previously drained terrain. The nonradial direction of neighboring drainage networks imply disequilibrium between that fluvial system and the present lake. In comparison, spectrally distinct rings surrounding Ontario Lacus, interpreted as paleo-shorelines by Barnes et al. (2009a), suggest a long-term reduction in base level. In the north polar region, partially filled and empty lakes are not seen poleward of 77° and are almost always found within close proximity of each other. A notable exception is between 120°W and 160°W, where empty lakes are found in the absence of partially filled lakes. This region is also characterized by a large density of small isolated lakes with comparatively smooth borders and relatively sharp shoreline contrast. These observations have led Hayes et al. (2008) and Mitchell et al. (2009) to suggest that this area may be a network of seepage lakes

Table 2.1 *Lacustrine feature coverage statistics normalized by observed SAR coverage. North and south polar regions are defined as latitudes poleward of 55°*

Feature type	Global	North	South	Median area
SAR swath coverage	47.8%	56.2%	62.8%	N/A
Dark/filled	1.2%	10.5%	0.4%	77 km^2
Granular/partially filled	0.1%	0.7%	0.1%	143 km^2
Bright/empty	0.2%	1.2%	0.4%	341 km^2

interacting with a subsurface alkanofer, the hydrocarbon analog of an aquifer on Earth. Many of the smaller lakes also have bright rims in SAR images, suggesting that they are steep-sided depressions that are only partially filled (Hayes et al., 2008).

The morphology of lacustrine features in the south is notably different from that in the north, lacking both the large maria and clustered groupings of smaller lakes that are characteristic of northern terrain. Although not included in the mapping statistics, also of note are dark areas, morphologically similar to terrestrial mudflats (Lopes et al., 2010), found near (210°W, 80°S) and (0°W, 75°S). Limited topography from SAR-Topo measurements (Stiles et al., 2009; Zebker et al., 2009) suggests these features, along with the lakes, are located in the lowest elevations of the south polar region. When referenced to estimates of Titan's geoid (Iess et al., 2010), these areas have comparable elevations to the north polar maria shorelines reported in Kirk et al. (2012).

The relative elevation of lake shorelines can provide information regarding the importance of subsurface connectivity and transport in Titan's methane cycle. The large northern seas, or maria, are located in the lowest elevations of the north polar region and their shoreline elevations are self-consistent to within the ~150 m absolute accuracy of the topography data presented in Kirk et al. (2012) and Stiles et al. (2009). Although this does not conclusively show that the maria shorelines share an equipotential surface, it is not inconsistent with such a hypothesis. Further support for shared maria shoreline elevations is provided by the apparent connection between the largest maria, as viewed by ISS and VIMS (Turtle et al., 2009; Sotin et al., 2011). The areas of empty and partially filled lakes, which flank the maria to the south, lie about 400 m above the maria shorelines. The area of small lakes located between 120°W and 160°W in the north polar region lies 600 to 800 m above the maria shorelines, producing a potential hydrologic head for subsurface transport. The regional slope between the small lakes and the maria is ~0.04 degrees. Empty lakes observed in varying locations throughout the north polar region are seen as ~150 to 300 m depressions by all three topographic techniques. The 1 km variation in topography near the northern maria may also help to generate lake-effect clouds, suggested by Brown et al. (2009) using VIMS.

Although lakes near the maria exhibit elevations that are arguably consistent with the sea shorelines, distant lakes, on the other hand, are topographically elevated by 400 to 800 m. In some cases, these lakes even lie in a state of local hydrologic disequilibrium. The *Cassini* Solstice Mission (September 2010–September 2017) includes Titan passes designed to observe these areas again to see how they evolve temporally. The evolution of lakes of different sizes in these areas can provide constraints on the properties of the local porous regolith and the importance of subsurface transport in Titan's hydrologic system (Hayes et al., 2008). Under simplifying assumptions, small lakes are dominated by interaction with the subsurface (infiltration), whereas large lakes are dominated by interaction with the atmosphere (evaporation). An early attempt to estimate the depth of Titan's lakes was performed by Lorenz et al. (2008a), who used the correlation between lake size and depth for Earth's twenty largest lakes to suggest that small lakes (area ~$10^2 km^2$) had depths of ~10 m and the largest seas (area ~$10^5 km^2$) had depths of ~300 m. Using these values, Lorenz et al. (2008a) estimated that the total volume of liquid hydrocarbon on Titan's surface was between 30,000 and 300,000 km^3, or between 4 percent and 40 percent of the atmospheric methane

inventory. Based on these results, Lorenz et al. (2008a) concluded that the lakes alone could not balance photolytic loss for more than a few to ten million years.

Compared with water, liquid hydrocarbon (methane/ethane) is greater than three orders of magnitude more transparent to microwave radiation. The penetration depth of microwave may be related to the loss tangent, $\tan\Delta$, of the material, which is the ratio between the imaginary and real components of the dielectric constant. Assuming a dielectric constant of $(1.75 + 0.002i)$ for liquid hydrocarbon on Titan (Paillou et al., 2008b), the two-way Ku-band 1/e attenuation depth is ~1 m, as compared to ~0.3 mm for 15°C water on Earth. Furthermore, about 99 percent of the radiation is transmitted through an air/hydrocarbon (methane/ethane) interface, as compared with about 40 percent for an air/water interface (average over 10°–50° incidence). Therefore, unlike water on Earth, the *Cassini* RADAR can potentially be used to probe the depth of partially filled lakes on Titan.

To estimate the loss tangent of liquid hydrocarbon under Titan conditions, Paillou et al. (2008b) made measurements of liquid natural gas, which is a hydrocarbon mixture of approximately 90 percent methane, and measured a loss tangent of 1.1×10^{-3} at *Cassini*-relevant wavelengths. Sen et al. (1992) measured the loss tangent of pure hydrocarbons, placing an upper limit of 10^{-4} on the loss tangent of pure methane or ethane. Hayes et al. (2010) analyzed the near-shore regions of Ontario Lacus and derived a loss tangent consistent with that of Paillou et al. (2008b).

Hayes et al. (2010) observed that radar backscatter decreased exponentially with distance from the shoreline at Ontario Lacus. This behavior is consistent with attenuation through a deepening liquid layer and, if the local slope is known, can be used to derive the loss tangent. An altimetry pass was acquired in December 2008 (T49) that intersected the Ontario Lacus at two points (Figures 2.7 and 2.12). By assuming that Ontario is liquid filled and that the slope just offshore continued into the near-shore region, Hayes et al. (2010) were able to derive a loss tangent of $\tan\Delta = 9.2 \pm 2.5 \times 10^{-4}$. Further assuming that the loss tangent was consistent throughout the lake, near-shore bathymetric slopes of additional regions around the shoreline were also determined. It should be noted, however, that the derived loss tangent from Hayes et al. (2010) is inversely

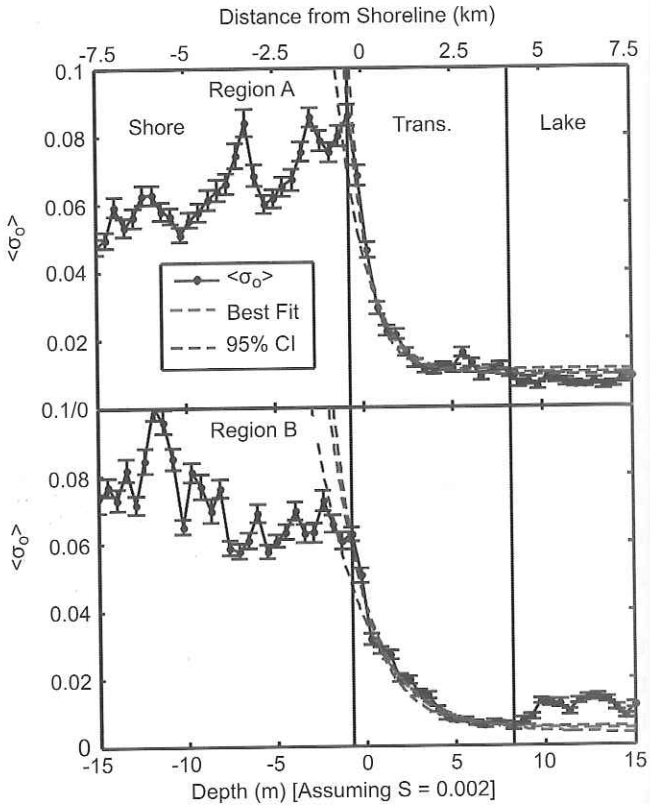

Figure 2.12 Along-shore averaged radar backscatter and model fits for Ontario Lacus. Regions A and B correspond, respectively, to the eastern and western intersections of the altimetry profile with the border in Figure 2.7. The red and brown lines represent the best-fit and 95% confidence interval models from Hayes et al. (2010). (See color plate.)

proportional to the slope at the intersection point between Ontario Lacus and the December 2008 altimetry pass. If the slope is not continuous across the shoreline, then the loss tangent would need to be scaled accordingly. Similar near-shore backscatter variations are observed on the southeastern shores of Ligeia Mare, suggesting shallow bathymetry slopes in this region as well.

SAR images of Ontario Lacus show consistent structure within the lake between multiple observations (Wall et al., 2010; Hayes et al., 2010). The fact that these structures are seen at two different times suggests that they represent variations in the lakebed as opposed to the lake surface, and further suggest that the depth of the liquid in these regions can be at most a few times the two-way absorption depth. Wye et al. (2010) modeled the depth in these regions by investigating a range of scattering properties for the lakebed and lake

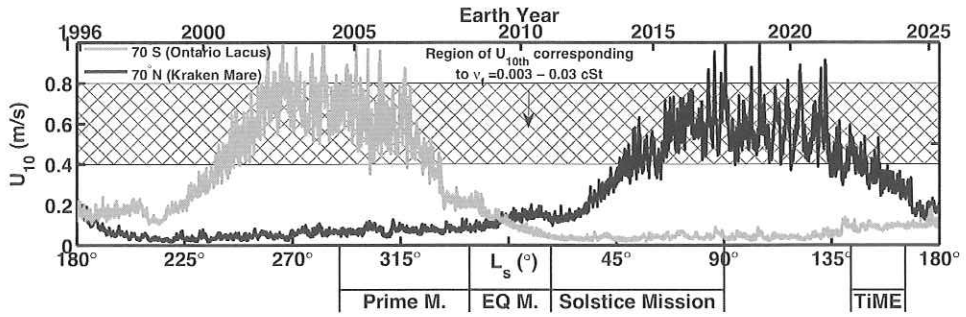

Figure 2.13 Daily averaged wind speeds at 10 m altitude from Schneider et al. (2012) using a three-dimensional idealized Titan GCM. Values represent the 95% quantile of the longitudinal distribution at 70°S (gray line) and 70°N (black line) for a given time after averaging over five seasonal cycles. The cross-hatched region highlights the expected range of threshold wind speeds for viscosities ranging between pure methane rain and the more complex mixtures discussed by Cordier et al. (2009). Wind speeds are expected to exceed threshold during the summer but remain below even the minimum threshold during each pole's equinoxes and winter.

surface. The estimated depth of the lake ranged from 1 m to 9 m, depending on the composition and structure of the lakebed. Clark et al. (2010) studied the properties of Ontario's surface scattering function using VIMS and determined that the ethane absorption path lengths of a few millimeters measured by Brown et al. (2008) require lake depths of 0.5 mm or the presence of a thick, "muddy," or particulate-rich, top layer. Another recent interpretation suggests expanses of the dark portions of the depression are not liquid covered, but rather an exposed, liquid-saturated floor (Cornet et al., 2012).

In addition to a topographic profile, the December 2008 altimetry pass also provided nadir backscatter measurements over Ontario Lacus. Wye et al. (2009) showed that the altimetry echoes from the lake were specular in nature and that the surface had a maximum root-mean-square surface roughness of 3 mm, suggesting no wave activity. More recently, Stephan et al. (2010) described images of a sun glint over a lake surface (later named Jingpo Lacus, or "mirror-lake") in the North Polar region acquired by VIMS. Barnes et al. (2011b) further analyzed the data to find that the RMS-slope had to be less than 0.25° during image acquisition, also suggesting little to no wave activity. In general, the observation that dark lakes are at or near the RADAR noise floor is further evidence for a lack of any substantial wind-waves (Notarnicola et al., 2009). These observations are intriguing given the predominance of aeolian features in the equatorial latitudes, which require winds capable of saltating sand size particles (100–300 μm) (Lorenz et al., 2006a). This apparent discrepancy may be caused by differences between the conditions required for wave generation on Titan and Earth. The physical parameters associated with exciting wind-waves on Titan were reviewed by Lorenz et al. (2010).

On Earth, the two most common models for predicting the exponential growth rate of gravity-capillary wind-waves are those of Plant (1982) and Donelan and Pierson (1987). Both predict threshold wind speeds, the point at which growth balances loss by viscous dissipation, to be between ~1.5 m/s and ~2 m/s (measured at 10 m), depending on water temperature (Donelan and Plant, 2009). Evaluating these models under Titan conditions suggests threshold wind speeds of 0.4 to 0.8 m/s for compositions varying between methane rain and the more complex mixtures suggested by Cordier et al. (2009), depending on liquid viscosity (Hayes et al., 2011b) (Figure 2.13). The reduced threshold is a result of Titan's increased atmosphere-to-liquid density ratio and reduced gravity and fluid surface tension. The observations of Ontario and Jingpo Lacus were acquired near equinox, when most GCMs predict wind speeds below this threshold (Hayes et al., 2011b) .

Observations planned during the *Cassini* Solstice Mission, however, will be acquired during the northern spring and summer, when wind speeds may exceed the predicted threshold. Once gravity-capillary waves begin to grow, gravity waves will soon follow, eventually leading to a fully developed sea if the fetch is large enough and liquid depths are greater than a few meters. For a given wind speed, Titan's reduced gravity will lead to significant wave heights about seven times

greater than those on Earth. However, the low wind speeds predicted on Titan suggest that the significant wave height will remain below ~0.6 m, which is below the maximum potential tidal amplitude of the largest seas (Lorenz et al., in press).

Potential explanations for the observed hemispherical dichotomy in Titan's lake distribution are discussed in Aharonson et al. (2009) and include seasonal effects, topographic differences between the poles, and energetic effects resulting from variations in solar insolation. Although seasonal effects may seem the most obvious, the paucity of both empty and filled lakes in the southern hemisphere points to a process with longer timescales. Geologically, the north polar region does not resemble a flooded version of the south. Furthermore, the empty lakes in the north are consistently observed to be 100 to 300 m depressions. Masking the signature of such a depression would be difficult over the 29.5-yr Titan season. A hemispheric topographic difference relative to the equipotential surface is possible. However, the global topography and gravity data available as of this publication do not support this theory (Zebker et al., 2009; Iess et al., 2010). In fact, the best-fit ellipsoid for the current data set suggests that the difference between northern and southern polar topography is an order of magnitude smaller than the topographic variation within the polar regions themselves (Figure 2.1(B)). A hypothetical impermeable subsurface boundary might alter the drainage properties of each hemisphere differently, but so far no evidence for such a boundary has been seen.

Aharonson et al. (2009) suggest that the asymmetry in lake distribution is caused by the asymmetry in Titan's season due to Saturn's eccentricity and obliquity. The solar longitude (Ls) of Titan's southern summer solstice is currently within 6° of Saturn's perihelion. Conversely, the northern summer solstice occurs within 6° of aphelion, when Titan is 1 AU further from the sun. Because of this geometry, Titan's southern summers are shorter and more intense than its northern summers, with a peak insolation difference of around 25 percent at the top of the atmosphere. GCMs show this energy difference, when propagated through the atmosphere, provides a forcing for net movement of both methane and less volatile species, such as ethane, to the north pole over tens of thousands of years (Schneider et al., 2012).

However, Saturn's orbital elements are not constant. The current situation was reversed ~32 kyr ago, with northern summer experiencing about ~25 percent higher peak insolation than the south. The variation of Saturn's orbital parameters are such that the seasonal asymmetry will reverse over periods of ~50 kyr, requiring Titan's polar surfaces to be modified on timescales of tens of thousands of years (Aharonson et al., 2009). Longer-period insolation cycles are also present, a situation analogous to Earth's Croll-Milankovitch cycles and the obliquity cycles of Mars (Figure 2.14). On those planets as well, the orbital oscillations are thought to drive large-scale variations in the distribution of their respective volatiles (H_2O and CO_2). Although the lack of observed craters in the polar regions of Titan is consistent with latitude-dependent resurfacing processes, the masking of empty lake depressions over orbital timescales remains a challenge. However, this hypothesis is consistent with the observed lake distribution, magnitude of dynamic changes observed by the ISS and RADAR instruments, and VIMS detection of ethane in Ontario Lacus, as ethane is 10^4 times less volatile than methane and would be expected as the remaining residual after much of the methane evaporated.

2.6 Fluvial processes

Titan is the second known solar system body on which sustained, channelized flows associated with atmospheric precipitation appear to have occurred in the geologically recent past. The occurrence of fluvial features provides several fundamental constraints on the characteristics of Titan's surface environment. It requires a surface material that can be eroded physically or chemically, a flow with sufficient duration and intensity that it is capable of eroding the surface, and a fluid sufficiently inviscid that it becomes concentrated in conduits that are much longer than they are wide. If the flow depth is much smaller than the relief of the landscape, such that the weight of the fluid is the main force driving flow, then the occurrence of fluvial features requires a mechanism that generates slopes at the solid surface, either through uplift or subsidence, or through gradients in erosion or aggradation of material, such as impact craters and ejecta. A detailed understanding of the fluvial features therefore promises to reveal much about the mechanical and chemical properties of the

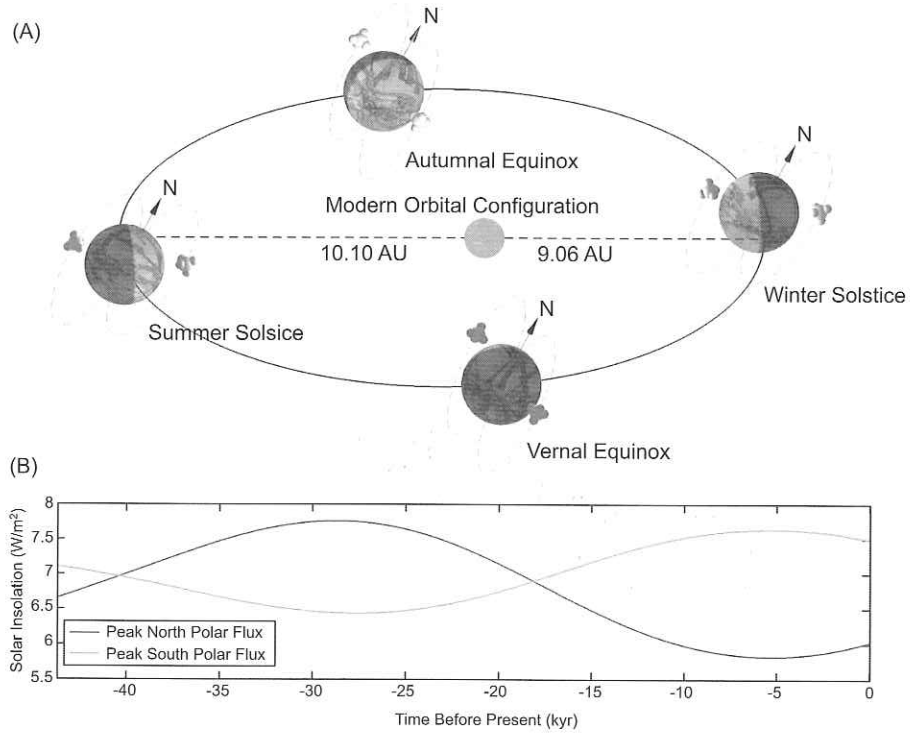

Figure 2.14 (A) Position of Titan's seasons relative to Saturn's orbit summer solstice current coincides with perihelion, resulting in a 25% peak insolation difference between south and northern summer (Aharonson et al., 2009). (B) Evolution of peak insolation in the north and south polar regions. As the orbital elements evolve, so does the insolation difference, and the expected latitudinal distribution of volatile hydrocarbons.

surface, the climate and weather that generate flows, and the mechanisms that produce topographic relief. Titan's fluvial landscapes will test our ability to understand landform development at a fundamental level that is not specific to gravitational acceleration, properties of the fluid and solid surface, large-scale deformation mechanisms, or rates of erosion and transport.

Previous reviews have covered various aspects of Titan's fluvial features, including their spatial distribution (Lorenz et al., 2008; Jaumann et al., 2008; Jaumann et al., 2009a; Langhans et al., 2011; Burr et al., 2013), the variability of their morphology (Lorenz et al., 2008; Lunine et al., 2008; Burr et al., 2009; Jaumann et al., 2009a; Lopes et al., 2010; Langhans et al., 2011; Burr et al., 2013), and their spectral characteristics (Langhans et al., 2011). The discussion here is organized around the processes that form the fluvial features, based on the characteristics summarized previously. Here, we discuss the inferences about formation processes that can be made based on these characteristics, and consider the most significant unknowns that currently limit our understanding of fluvial processes on Titan.

The view of Titan's fluvial features afforded by the *Cassini-Huygens* mission prompts three basic questions about formation processes, which concern the nature of the incision mechanism, the type of flow, and the flow magnitude. The first question is whether the fluvial valleys were created by mechanical or chemical erosion. (Although thermal erosion is a primary mechanism of super-glacial erosion on Earth [Parker, 1975], the evidence of widely distributed fluid sources rule out valley incision by erupted material, which would presumably be required to raise the temperature of the ice significantly above Titan's surface temperature.) Several studies have discussed the extreme insolubility of water ice in liquid hydrocarbons (Lorenz and Lunine, 1996; Perron et al., 2006), which makes erosion by dissolution unlikely unless the composition of the surface material differs substantially from pure water ice (containing a significant fraction of ammonia, for example). Nonetheless, it has recently been proposed that the

margins of high-latitude lakes may have been shaped by dissolution of an organic-rich surface layer (Stofan et al., 2007; Bourgeois et al., 2008).

The morphology of the fluvial networks offers an independent test of the chemical erosion hypothesis. The most salient characteristic of Titan's fluvial features is that they form continuous networks that span hundreds of kilometers. We are not aware of any terrestrial analogs in which large-scale, surficial fluvial networks are created entirely by dissolution, even where bedrock is highly soluble in water. This morphologic observation does not rule out chemical erosion, but it does suggest that mechanical erosion played a significant role. If future images with higher spatial resolution reveal an intricate network of discontinuous channels, pits, and collapse features covering the surface, the view that mechanical erosion has been dominant will have to be re-evaluated, but at present, there do not appear to be any morphologic features of the fluvial networks that require dissolution. In contrast, mechanical erosion is known to produce fluvial networks that are morphologically similar to those observed on Titan (Perron et al., 2006), and detailed assessments of the scaling of mechanical erosion and sediment transport processes to Titan's surface conditions have concluded that the mechanisms that drive bedrock channel evolution on Earth should be comparably effective on Titan (Collins, 2005; Burr et al., 2006).

The second basic question is whether Titan's valley networks were formed primarily by the incision of channelized surface flows, or by erosion driven by subsurface flow. It would be surprising if subsurface flow of hydrocarbons played no role in forming the valleys. In terrestrial drainage networks incised by channelized surface flows, both porous flow through the shallow subsurface and deeper groundwater flow usually contribute to the channel discharge. Only if Titan's surface were effectively impermeable would we expect to find valley networks incised purely by surface runoff.

A more dominant role for subsurface flow has been proposed, however: the morphology of fine-scale drainage networks to the west of the *Huygens* Probe landing site (Figure 2.15) has been cited as evidence of sapping erosion (Tomasko et al., 2005; Soderblom et al., 2007), in which the emergence of subsurface flow mechanically erodes material. The retreat of valley headwalls due to groundwater sapping in unconsolidated soil and sediment has been shown to generate valley networks with theater-shaped valley heads and short, wide tributaries with nearly orthogonal junction angles (Dunne, 1980; Howard, 1988; Schumm et al., 1995). The distinction between valley networks incised by channelized surface flows and sapping is important in the context of rainfall on Titan, because sapping could indicate a less direct role for atmospheric recharge. On Mars, where some of the younger valley networks have short, wide tributaries and theater-shaped valley heads, a similar argument has been used to question the role of rainfall (e.g., Malin and Carr, 1999; Gulick, 2001).

Terrestrial research has revealed the difficulty of inferring a significant role for groundwater sapping from valley morphology alone (Lamb et al., 2006). Sapping is known to occur in cohesionless or weakly cohesive sediment, but evidence of efficient sapping in bedrock is lacking, environments where surface runoff plays no role in valley development are difficult to find, and the morphologic characteristics commonly associated with sapping erosion can also be formed by floods (Lamb et al., 2008) or mass wasting of canyon rims (Lamb et al., 2007). If the surface material on Titan is highly permeable and is not strongly cohesive (a possibility discussed later in this section), it is likely that some sapping has occurred, but caution must be exercised in interpreting valley morphology. If higher-resolution imagery and topography become available in the future, it may be possible to use the forms of hillslopes bounding fluvial valleys to gauge whether sapping has played a substantial role in valley development (Perron and Hamon, 2012).

The third basic question is whether the fluvial features were created by catastrophic flows, or by sustained or repeated flows of smaller magnitude (again, mirroring the debate on martian fluvial systems). Valleys incised by catastrophic flows, such as the outflow channels on Mars or the Channeled Scablands of Washington State, have a number of distinctive characteristics: there are often large variations in valley width as the flow passes over irregular topography, the channel may split into multiple threads where it encounters major topographic obstacles, and the ratio of channel width to valley length is typically larger than for river channels. For catastrophic floods, the channel width and valley width may be the same. Flood-triggering mechanisms,

such as the breach of an ice dam, typically generate a flow that originates from a point source and receives no significant inputs along its course.

In contrast, the nearly uniform width, single-thread morphology, and large length-to-width ratio of many fluvial features on Titan indicate a noncatastrophic origin, with valleys incised by flows much narrower and shallower than the topographic features they gradually create. The presence of tributary networks that originate from many distributed sources is also consistent with smaller-magnitude flows fed by gradual atmospheric recharge. Sinuous features on Titan might be valleys created by meandering channels, which would also imply sustained or repeated flow, but it is important to note that channel sinuosity can develop through mechanisms other than a meandering instability, such as steering of the flow around topographic obstacles as it navigates a rough surface.

Beyond these basic observational constraints, significant questions remain about the development of fluvial landforms on Titan. Here, we list some of the most fundamental unknowns and discuss the implications for our understanding of Titan's surface. Some of these questions could potentially be addressed using *Cassini-Huygens* observations, whereas others must await future missions that reveal the surface in finer detail.

The extent to which Titan's landscape is dissected by fluvial networks, in terms of both areal coverage and drainage density, is important for constraining Titan's climate and hydrology. The fact that areas within the best-resolved location, the *Huygens* landing site (Figure 2.15), are dissected by fine-scale valley networks that are not resolved by *Cassini* RADAR (Jaumann et al., 2009a) suggests that Titan's landscape could have a pervasive network of fluvial features that is currently invisible to us. Experience from terrestrial settings serves as a reminder that RADAR images can enhance features that are topographically insignificant while obscuring features that are topographically prominent (Black et al., 2012; Burr et al., 2013).

Fluvial erosion is ultimately linked to relief production; and hence a record of how much erosional exhumation has occurred on Titan could help discriminate between a history of continuous relief production and a history of isolated relief-producing events. In some regions, such as the areas surrounding the north polar lakes, the visible portions of fluvial networks are narrow, with tributaries concentrated close to the main stem. Landscape evolution models show that this is qualitatively consistent with the early stages of dissection of a rough surface, suggesting that these regions have undergone little erosion since the most recent relief-producing event (Black et al., 2012). Any question about cumulative erosional exhumation is closely related to the question of what produced the limited relief currently observed on Titan's surface, and whether the relief production was separated in time from the main erosional phase (as would be expected if the relief was produced by impacts or cryovolcanism [Mitri et al., 2008]), or whether mechanisms other than erosion (such as dynamic topography, viscous deformation [Perron and de Pater, 2004] or tectonism [Radebaugh et al., 2007; Mitri et al., 2008, 2010]) continue to change that relief over time.

An opportunity to quantify the magnitude of regional fluvial erosion is presented at the shores of Kraken Mare, at and near the island of Mayda Insula imaged by SAR. denoised RADAR images reveal a landscape dissected by fluvial features draining into the lake (Lucas et al., 2011). The region was imaged by two overlapping passes, enabling a stereo-derived topographic model. The digital elevation model (DEM) from denoised images is similar to, but has a greater fidelity and lower errors than, the one derived from the original images. The DEM is shown in Figure 2.16. The elevation hypsogram shows a bench in the topography at an elevation of approximately −240 m. The shoulder in the distribution is seen in the DEM derived from noisy images, and is even more distinctive in the DEM derived from denoised images. The elevation range of the bench between −500 m and −240 m corresponds closely to the region of the shorelines of Kraken Mare, at the perimeter of Mayda Insula and the near-shore regions on land, indicating that this region has been modified by fluvial/lacustrine processes near the shore. In addition to the observations of valleys that incise the terrain at least superficially, a volumetrically significant signature is seen when examining the topography. The area in the hypsogram missing relative to the unmodified topography corresponds to the volume of material redistributed by the combination of erosion and deposition. This volume is estimated to be ~2 km^3 within Mayda Insula, which is equivalent to roughly

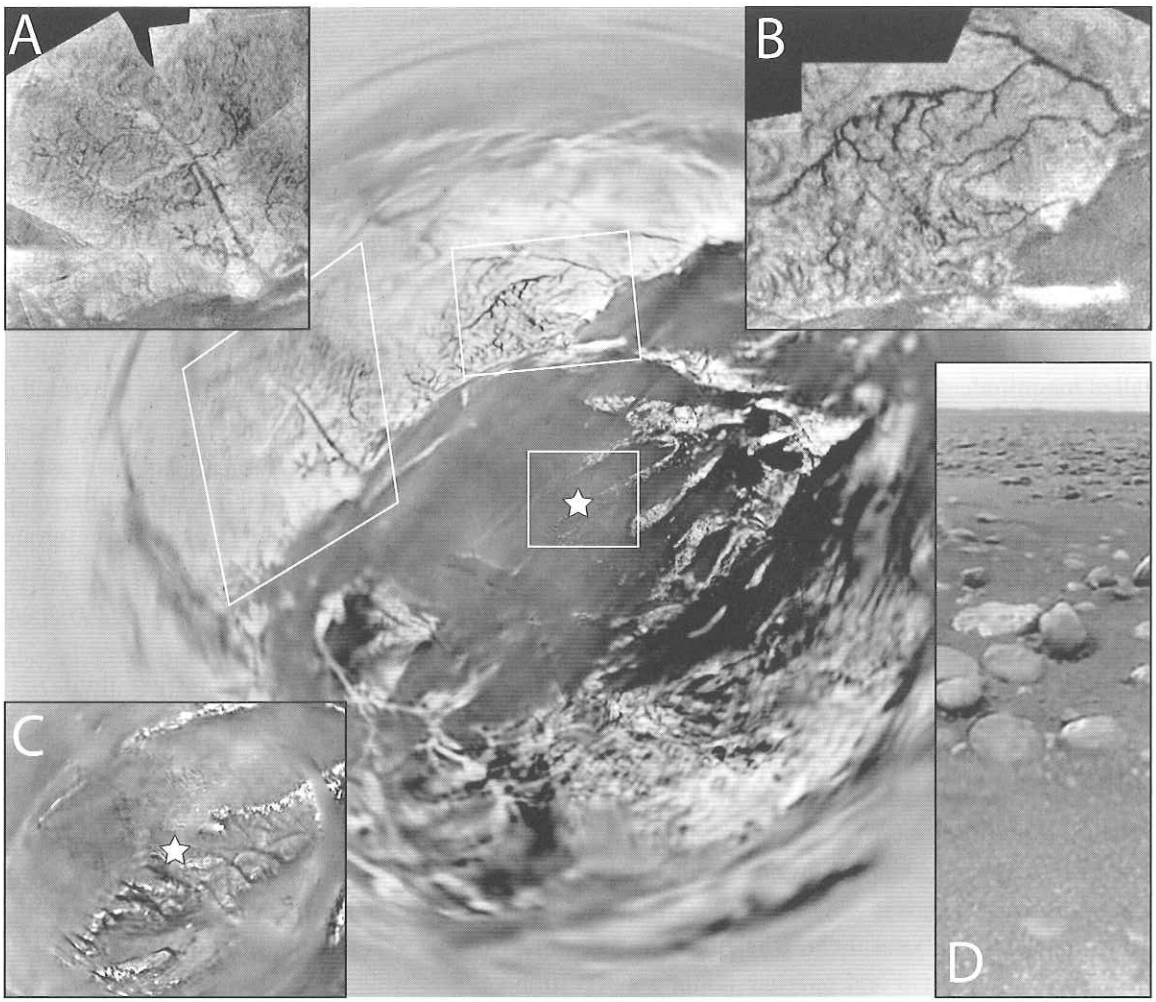

Figure 2.15 Image mosaics from the *Huygens* Descent Imager and Spectral Radiometer (DISR) of features around the *Huygens* probe landing site, at approximately 10°S, 192°W. Background: stereographic projection of the view from 6 km above the surface, centered on the landing site, marked with a star. North is up. Scale varies across image. White boxes show the approximate extents of insets (A)–(C). Insets: (A) Western drainage networks. Image width is approximately 8 km. (B) Northern drainage networks. Image width is approximately 6 km. (C) Stereographic projection of the landing site from 600 m above the surface. Image width is approximately 2 km. (D) View from the landing site, looking toward the horizon. Diameter of the largest clasts in middle distance is roughly 15 cm. All images courtesy of NASA/JPL/ESA/U. Arizona. Reproduced from Burr et al. (2013).

1 m of spatially averaged erosion in the affected area, a value consistent with independent estimates of spatially averaged fluvial erosion (Black et al., 2012). Quantifying the geomorphic work performed on the topography enables comparison of the effect of fluvial erosion on the terrain with that on Earth and Mars and highlights that fluvial valleys on Titan modify the terrain volumetrically, beyond their planform appearance in images.

As discussed previously, there are currently few constraints on the geometry of Titan's fluvial channels (as distinct from the fluvial valleys that contain the channels). A major distinction that has not yet been made is whether fluvial channels are dominantly erosional, or whether there are also self-formed alluvial channels created through sediment deposition as discussed earlier and suggested by Lorenz et al. (2008). The plan-form and cross-sectional geometry of alluvial channels would constrain other aspects of the surface environment. If channel banks are built of cohesionless sediment and sediment loads are large, braided channels that occupy a larger fraction of the valley width may be common. If organic particles derived from aerosols provide enough cohesion to stabilize banks and bars, on the other hand, single-thread, meandering channels may be more widespread. Channel forms should also bear a record of climate, including the

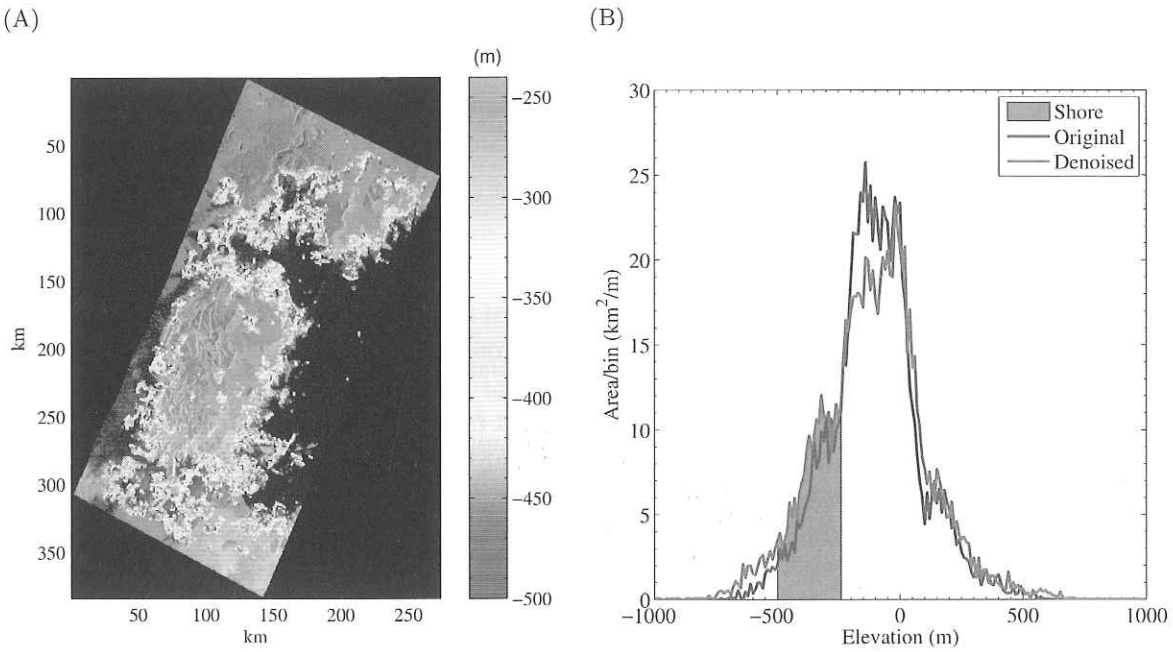

Figure 2.16 (A) Denoised SAR image of Mayda Insula in Kraken Mare (310°W 78°N). A DEM was derived from denoised SAR image pair obtained in February and April 2007 (T25 and T28). (B) Hypsogram of elevations indicating a bench in the topography that corresponds to the near-shore regions of the island and surrounding topography. The indicated region (gray) is highlighted by the color-coded topography in the map, showing the correspondence. The elevations are measured relative to a local reference. (See color plate.)

magnitude and frequency of flows. If Titan's climate is such that rare, large-magnitude events are the rule (Hueso and Sánchez-Lavega, 2006), the hydraulic geometry of channels (Parker, 2005) may be significantly different from that on Earth.

Even with constraints on erosion and sediment transport from the morphology of fluvial features, there will be significant uncertainty about the rate and mechanism of fluvial erosion without better knowledge of the mechanical, chemical, and hydrologic properties of the surface material. Questions of particular interest are whether any of the solid materials present at the surface can dissolve in methane or ethane, and how rapidly cold ice erodes when subjected to impact wear by sediment. Laboratory experiments are beginning to provide measurements of the mechanical properties of very cold ice (Polito et al., 2008; Litwin et al., 2010), but such measurements must ultimately be paired with more detailed observations of Titan's surface materials to constrain mechanisms and rates of fluvial erosion. A related problem is that the origin, production rate, and physical properties of surface sediment remain uncertain. Knowledge of these factors is critical for distinguishing between probable fluvial erosion mechanisms (such as abrasion by suspended load, wear by saltating bedload, or plucking that is largely independent of the sediment load) (Burr et al., 2013), for estimating whether channels are incising into consolidated material or armored with a mantle of sediment, and for characterizing the hillslope response to channel incision.

Even if Titan's surface is extensively dissected by fluvial valley networks, it is likely that fluvial channels occupy a small fraction of the landscape, with the remainder of the topography consisting of hillslopes. The question of how hillslopes respond to fluvial incision is critical, because hillslope erosion and transport control the sediment supply to channels. Terrestrial analogs suggest two endmember scenarios: slopes mantled with granular material, or slopes of bare "bedrock" (i.e., consolidated material). In the former scenario, hillslope topography could be shaped by gradual downslope creep of the granular material. But on Earth, processes that weather rock to generate regolith and then transport the regolith through dilational disturbance are driven largely by bioturbation (Black and Montgomery,

1991; Gabet et al., 2003; Dietrich et al., 2003; Dietrich and Perron, 2006). There are examples on Mars of smooth, regolith-mantled hillslopes generated by abiotic processes (Perron et al., 2003; Dietrich and Perron, 2006), but these slopes were presumably not subjected to rapidly lowering boundaries, as hillslopes bounded by incising channels typically are. Thus, unless there are mechanisms that both weather the surface to generate granular material and cause disturbances that transport that material downslope, it is likely that hillslopes adjacent to fluvial channels on Titan are dominated by bare bedrock, erode by repeated landslides, and have steep slopes set by a balance between gravitational stresses and material strength (Schmidt and Montgomery, 1995; Montgomery and Brandon, 2002; Larsen et al., 2010). A definitive answer to the question of how hillslopes on Titan respond to fluvial incision will require imagery and topography with a resolution finer than the scale of fluvial dissection (meters to a few tens of meters).

In summary, it is likely that fluvial processes on Titan are dominated by mechanical incision of channels by flows sourced from atmospheric recharge. Moreover, some of these channels have incised deeply enough to generate a hillslope response, forming valleys that are visible even in images with pixel sizes of hundreds of meters. Several major uncertainties about fluvial processes remain, including the physical characteristics of the material being eroded, the morphology of the channels themselves, and the geographic extent and cumulative amount of fluvial erosion. Some observations suggest that fluvial exhumation of the current landscape has not been extensive: fluvial networks, though occurring over a wide range of geographic locations, appear to be patchy and limited in spatial density; moreover, the shapes of prominently visible fluvial networks in some regions suggest a strong influence of initial topography, as opposed to networks shaped by feedbacks among competing drainage basins (Black et al., 2012; Perron and Fagherazzi, 2012). There are three plausible explanations: (1) Titan's climate has only recently evolved to a state in which atmospheric recharge and surface flows of liquid hydrocarbons occur; (2) the apparent limited occurrence is an artifact of image characteristics or limited image resolution, and the surface is in fact extensively dissected by fluvial features; or (3) Titan's surface topography was recently (relative to the rate of the hydrocarbon cycle) reshaped by some other process, and fluvial incision has had little time to respond. Given the invisibility of the fluvial features at the *Huygens* landing site in coarser resolution images (Jaumann et al., 2009a) and the general possibility that topographically prominent features are obscured in RADAR images (Black et al., 2012; Burr et al., 2013), it seems likely that image characteristics are at least part of the reason for the apparently patchy dissection. This observational bias does not explain the morphology of fluvial networks that are visible, however. A likely scenario is that fluvial networks are actively dissecting a landscape that has not yet undergone extensive erosional exhumation, for either the first or third reason given earlier. That is, fluvial networks have incised enough to alter the appearance of the landscape over large areas, but the spatially averaged erosion is still a small fraction of the initial relief.

2.7 Seasonal processes

As the number of overlapping Titan fly-bys increases during the *Cassini* prime and extended missions, it becomes feasible to study not only the morphology and distribution of surface features, but also their temporal variability. Thus far, the majority of surface changes has been observed in the south polar region and is attributed to evaporation and/or infiltration of lacustrine features during southern summer. There have been no definitive changes observed in the north polar region through the end of the *Cassini* Equinox Mission (June 2008–September 2010). However, fluvial features are observed at all latitudes, suggesting that rainfall occurs at all latitudes.

Equatorial region: Since orbital insertion in 2004, two major low-latitude equatorial cloud events have been observed. Schaller et al. (2009) reported an event centered at ~247°W that occurred in April 2008 and Turtle et al. (2011a) discuss a similar event at ~320°W that occurred in September 2010. The 2010 event was followed up by multiple ISS observations acquired in October showing an area greater than 500,000 km^2 darkened in the wake of the storm, whereas observations obtained in November show the region brightening once again (Turtle et al., 2011a). These changes were interpreted as widespread methane rainfall wetting and/or ponding on the surface,

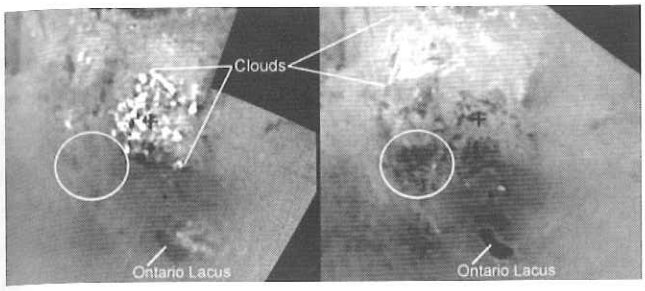

Figure 2.17 ISS mosaics of Titan's south pole acquired in July 2004 (left) and June 2005 (right). Arrakis Planitia is circled, where dark features have been interpreted to be liquid deposits that appeared between these two observations as a result of rainfall from a large cloud outburst that occurred in fall 2004 and later evaporated or infiltrated before subsequent observations. Modified from Turtle et al. (2009).

consistent with the atmospheric model of Mitchell (2008), who predicted equatorial rainstorms near equinox (August 2009).

South polar region: Turtle et al. (2009) and Turtle et al. (2011b) discuss albedo dark features that appeared in the south polar region between ISS observations acquired in July 2004 (Rev00) and June 2005 (Rev09) as shown in Figure 2.7. The primary area of observed change, Arrakis Planitia, has an area of ~30,000 km^2 and is located near (80°S, 120°W). In June 2005, Arrakis Planitia consisted of a collection of ISS albedo dark features that were interpreted by Turtle et al. (2009) as liquid deposits (Figure 2.17). The initial observations of the region in July 2004, however, showed that these features had similar albedo to their surrounding terrain. An extensive south-polar cloud system was detected in October 2004, suggesting that the terrain darkening may have been caused by surface liquid. Subsequent SAR images of the area obtained in December 2008 (T49) show no evidence for surface liquid, suggesting that any liquid present in June 2005 had since evaporated into the atmosphere or infiltrated into the subsurface (Turtle et al., 2011b). In addition, the border of Arrakis Planitia, as observed by ISS in June 2005, correlates with the morphologic boundaries of mountainous terrain and topographic depressions observed by RADAR (Hayes et al., 2011a). Turtle et al. (2011b) also observed potential shoreline recession at Ontario Lacus, although the later observation acquired in March 2009 (T51) is of poorer resolution than the image obtained in June 2005 (Rev09).

SAR images of Titan's south polar region were acquired during 10 fly-bys dating between September 2005 and January 2010. The largest baseline for observing potential change among these observations is ~2 years. Hayes et al. (2011a) analyzed overlapping SAR swaths in the RADAR data set and found that repeat images of the south acquired in 2007 and 2008/2009 contain lacustrine features that disappeared between observations. These transient features showed a tenfold increase in radar return, which was determined to be inconsistent with geometric effects and suggested temporal variability. Hayes et al. (2011a) used a two-layer scattering model to explain the observed backscatter variations and estimate an average drop in liquid depth of ~0.6 m/yr assuming a loss tangent consistent with Paillou et al. (2008b) and Hayes et al. (2010). The modeled loss rates are inversely proportional to the assumed loss tangent and ignore the effect of a dielectric contrast. When a lake dries completely, the dielectric interface changes from liquid hydrocarbon/lakebed to air/lakebed. Depending on the structure and saturation level of the regolith, even a thin layer can act as an antireflection coating and hence reduce the change in liquid depth required to explain an observed backscatter change upon drying. Hayes et al. (2011a) also investigated an apparent shoreline recession between ISS and RADAR images of Ontario Lacus. The recession (Figure 2.17), which occurred between June 2005 (Rev09) ISS observations and July 2009 (T58) SAR data, was shown to be inversely proportional to the near-shore bathymetric slopes estimated by Hayes et al. (2010). This relationship is expected if there were a constant reduction in lake depth, and Hayes et al. (2011a) derived a uniform reduction of 1 ± 0.3 m/yr between solstice and equinox. The absolute magnitude of the shoreline recession derived depends on the assumed liquid loss-tangent, as well as the determination of the position of the diffuse ISS shoreline. The detection of changes across multiple instruments is challenging, as demonstrated in an independent analysis by Cornet et al. (2010), which suggests that, to within errors, there is no significant change in the shoreline of Ontario Lacus.

North polar region: Since the first detection of northern lakes in SAR data acquired in July 2006 (T16) (Stofan et al., 2007), the north polar region has been imaged by seven additional SAR passes dating between September 2006 (T18) and December 2009 (T64). All

but one of these observations were obtained over the course of a nine-month period between July 2006 and May 2007, presenting only a short baseline for change detection relative to Titan's 29.5-year seasonal cycle. The most recent observation of the north polar region (T64), acquired in December 2009, provides up to a 3.5-year baseline between overlapping passes. Although there are differences in the appearance of lacustrine features imaged in both T64 and previous passes, analysis by Hayes et al. (2011a) suggests that, to within observational errors, they can all be explained by variations in viewing geometry. More recent observations of the north polar region by VIMS acquired in early 2010 also suggest that there has been no surface change (Sotin et al., 2011). Recent model results (Schneider et al., 2012; Mitchell, 2008) appear consistent with a lack of demonstrable surface changes in the north during winter, but surface changes remain difficult to exclude in the presence of observational effects.

2.8 Tectonic processes

Evidence for various compressional and extensional tectonics has been reported for Titan. More generally in icy satellites, multiple potential driving forces for tectonism exist; these include tides, despinning, nonsynchronous rotation, polar wander, volume change due to thermal expansion or phase change, convection, and diapirism. On Titan, the scale of tectonic processes observed is limited to those recorded in features discernible in the imaging data sets, typically on the order of, or greater than, 1 km (with the exception of smaller possible faults suggested to control the drainage system in the *Huygens* descent images [Soderblom et al., 2007; Figure 2.15]). At this scale, mountain ranges dominate the tectonic landforms. Evidence for tectonic activity is obscured and erased by resurfacing mechanisms, as also evident in the paucity of craters. Hence, overall, studies of tectonic processes on Titan are restricted relative to those on other icy satellites.

The mountain ranges seen on Titan typically appear radar bright, isolated blocks or chains (Figure 2.2). Using radarclinometric techniques, it is possible to estimate the geometry of the mountains; they exhibit heights of several hundreds of meters, up to ~2 km, generally with gentle slopes (Radebaugh et al., 2007). Possible formation mechanisms have been suggested by Radebaugh et al. (2007), and include crustal compressional tectonism and upthrusting of blocks, extensional tectonism and formation of horst-and-graben, deposition as blocks of impact ejecta, or dissection and erosion of preexisting layers of material. Perhaps the most dramatic known tectonic structures on Titan are seen in the Xanadu region. Unique signatures discriminating these mechanisms are not found in the data. Hence, for the Xanadu region, it is difficult to reject even the simplest picture in which diffuse extensional stress localizes on faults, with tilted blocks generating relief and fluvial erosion modifying the topography. A large impact event has been invoked to explain the anomalous properties of the Xanadu region (Brown et al., 2011), a scenario in which the interpretation of the tectonic setting would be further altered.

From the global perspective, models of the interior (Mitri et al., 2010) consider the effect compressional stresses on an icy shell overlying a liquid layer. In this model, global contraction due to the secular cooling of the body forces lithospheric shortening. The resulting tectonics express as folds with wavelengths of tens of kilometers and amplitudes of several kilometers, fitting with the observations. The contraction is greater if the liquid layer contains a large fraction of ammonia, and smaller if salts are dissolved. The notion of contraction being the dominant stress regime in generating tectonics is supported by examples on Titan in which mountains occur in areas that are themselves elevated with respect to their surroundings.

2.9 Cratering processes

As on other solid bodies, impact craters on Titan probe the target materials and their number density reveals the surface age. The thick atmosphere decelerates and breaks up projectiles up to ~1 km scale (Ivanov et al., 1997), which on an airless comparable body would result in craters up to ~10 km in diameter. The remaining impactors that reach the surface result in an observed crater population (Wood et al., 2010; Neish and Lorenz, 2012) that indicates a relatively young surface age, of 200 million years age according to some models (Artemieva and Lunine, 2005), or up to 1 Ga according to other models (Korycansky and Zahnle, 2005). The observed size-frequency distribution of craters (Figure 2.18A) has craters larger

than 35 km more abundant than in theoretical models, and craters smaller than 35 km more sparse (Lorenz et al., 2008b; Neish and Lorenz, 2012). The difference in abundance relative to models indicates that the larger craters may be preserved from a more distant past than smaller craters, which are preferentially erased by erosion and burial. Interaction with the atmosphere, ablating and decelerating projectiles, may also account for the deficit in small craters in comparison to models. Finally, with an imaging data set of resolution comparable to the smallest features mapped, the small craters are most difficult to identify.

The geographic distribution of craters is not random (Figure 2.18B). A prominent concentration of craters appears over the region of Xanadu, with a crater density two to nine times greater than in the rest of Titan (Wood et al., 2010). Areas covered by dunes exhibit a paucity in craters. Dunes occasionally encroach on crater ejecta deposits, such as in the case of Ksa (30 km diameter) or Momoy (40 km diameter). The density of craters decreases with latitude, with a significant paucity of craters in the high latitudes. Craters in the northern high latitudes may be partially obscured by the liquid of the abundant lakes and seas, but this cannot account for the deficit in craters in the south. One possibility is that the migration of liquids from pole to pole responding to climate variations is responsible for the paucity of craters in the high latitudes, in analogy with latitude dependent erosion rates on Earth, also driven by astronomically forced glacial cycles.

Using the Kolmogorov-Smirnov (KS) test, the null hypothesis that the observed latitudinal distribution of craters resulted from a uniform distribution within the area covered by SAR images can be rejected with a confidence of 0.988. If the analysis is restricted to only craters of high certainty, then the null hypothesis can be rejected with a similarly high probability of 0.993. Figure 2.18(B) shows the geographic distribution of craters, as well as their latitudinal distribution function. All the craters at latitudes poleward of 60°N are identified with lower confidence classification and are relatively small (<10 km). The paucity of craters at high latitudes for the entire data set is statistically robust; if only the craters with the most certain identification are included, the trend is even more pronounced.

Combined observations by VIMS and RADAR reveal additional information on the geology of Selk

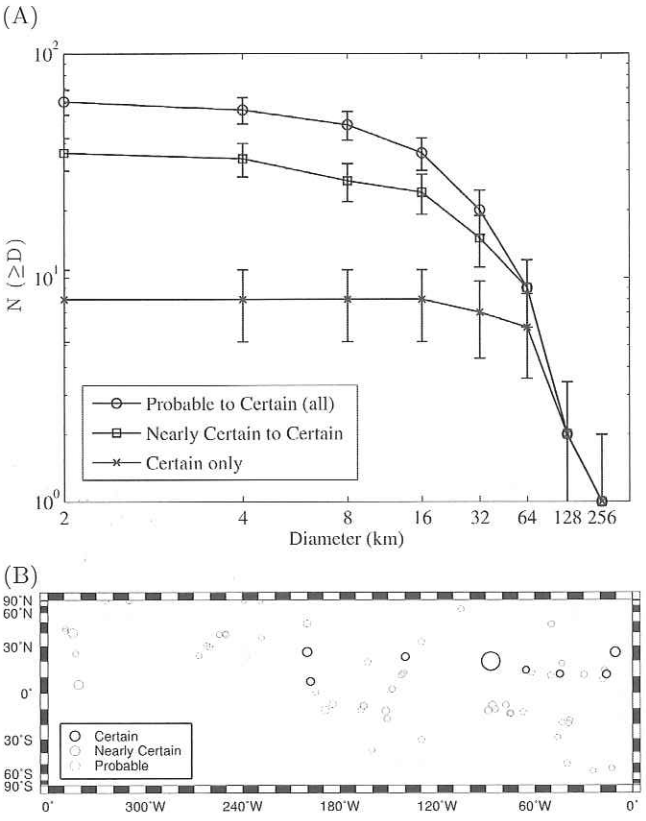

Figure 2.18 (A) Size-frequency distribution of craters, based on identification with confidence classes of Wood et al. (2010). (B) Geographic distribution of the same set of impact craters in an equal-area projection, highlighting paucity at high latitudes.

crater (Soderblom et al., 2010). With a rim crest of 90 km in diameter, a floor 60 km in diameter, and a terrace zone 10 to 15 km in width, the geometry of this bright-rimmed crater appears similar to comparable craters on other icy satellites. Structural control is evident in the polygonal morphology of the crater. Interaction with aeolian processes results in fluting of the interior rim walls and dunes encroaching on raised structures from the southwest. Fluvial processes channelize portions of the exterior rim deposits, leaving what are interpreted as sedimentary water ice deposits on the basis of their VIMS spectra (Soderblom et al., 2010).

2.10 Cryovolcanic processes

The search for cryovolcanic features on Titan is partly motivated by the desire to identify a mechanism for resupplying atmospheric methane (Atreya et al., 2006), whose photochemical lifetime is of order 10 Myr. Other

gases, such as ^{40}Ar, may also require subsurface release to the atmosphere. However, the existence of such features on Titan is still the subject of some debate. Favorable conditions for the persistence of cryovolcanism are thought to exist on Titan (Chapter 1) and early *Cassini* data from both VIMS and RADAR suggested several features produced by cryovolcanism to be present on the surface (Sotin et al., 2005; Elachi et al., 2005; Lopes et al., 2007). However, new data imaging some of these features, such as Ganesa Macula and Tortola Facula, showed that the initial interpretations of their cryovolcanic origins are questionable. This, at least in part, led Moore and Pappalardo (2011) to suggest that all known putative cryovolcanic features could be explained in terms of exogenic processes and that Titan could be thought of as "Callisto with weather" – that is, an icy world with little or no expression of internal processes at the surface. Subsequently, new RADAR data of Sotra Facula, a feature previously interpreted as cryovolcanic (Lopes et al., 2010), allowed a detailed topographic map to be made using overlapping SAR passes (Kirk et al., 2010). The topography (Figure 2.8) revealed the Sotra Facula region to be the strongest yet candidate for a cryovolcanic feature on Titan (Lopes et al., 2011). At present there is still no consensus on whether cryovolcanic features are present on Titan, but there is agreement that cryovolcanism is not ubiquitous and that the Sotra area is among the best candidates known for consideration. A description of the various candidate cryovolcanic features proposed and possible interpretations (Lopes et al., 2011) is summarized in Table 2.2. These features do not appear to be geologically young, but the possibility that activity is ongoing, perhaps in the form of outgassing such as that suggested by Nelson et al. (2009a,b), remains open.

The region known as Sotra Facula is the strongest cryovolcanic feature candidates to date. Sotra Facula was observed in SAR mode in two fly-bys during February and April 2007, respectively (T25 and T28). It was interpreted by Lopes et al. (2010) as a cryovolcanic edifice consisting of a partial depression ~30 km in diameter, adjacent to a relatively steep-sided mountain or dome ~40 km across. Lopes et al. (2010) also described a bright-edged lobate unit interpreted as a flow ~180 km long, extending to the north of the edifice. RADAR stereogrammetry (Kirk et al., 2012), obtained from the crossover swaths T25 and T28, revealed details of the region's topography, showing that the mountain at the southern end is ~1 km high and the adjacent depression is ~1.5 km deep and oval in shape rather than circular (therefore unlikely to be of impact origin). A second major peak, also ~1 km high, is found in a larger area of flowlike textures to the north of Sotra Facula itself, and separated from it by a 200-km-wide band of dunes. The flows are generally subdued in elevation, with thicknesses typically no greater than 100 m, but the flow area contains a previously unsuspected high terrain in the form of a 40-by-70 km ovoid with outer rim up to 0.8 km high and interior depressed below the surrounding terrain. The three areas of highest elevations are aligned in a NNE trend, to which the long axis of the middle ovoid is roughly parallel.

The topography, combined with SAR imaging and VIMS data, suggests that the Sotra Facula region is an area of multiple cryovolcanic features (Lopes et al., 2011). The interpreted features include two volcanic mountains, a deep noncircular depression associated with the southernmost mons, a flow that appears to emerge from this mons, other noncircular depressions between the two montes, and a series of flows surrounding the northern mons. Of particular interest is the fact that the area is devoid of fluvial features, making a fluvial origin for the flows unlikely. Moreover, the dune field that lies between the two montes indicates that this is a dry region. The fact that the depressions are not circular makes an impact origin unlikely, and there is no evidence of any impact ejecta blanket surrounding the depressions. Furthermore, the occurrence of Titan's deepest known depression and several lesser depressions in such close proximity to some of the most substantial mountains on Titan make it unlikely that impacts, so rare elsewhere on Titan, could explain these features.

If cryovolcanism has happened on Titan, how did the cryomagma get to the surface and what was the character of the eruptions? Lorenz (1996) discussed the possibility of finding cryovolcanic features on Titan, predicting that such features, if present, would be different from those on other satellites such as Triton, because the presence of a thick atmosphere on Titan would suppress the vesiculation of bubbles in a

Table 2.2 *Candidate cryovolcanic features and their interpretations*

Feature name and center location	Description	Proposed interpretations	Current interpretation: cryovolcanic feature?
Ganesa Macula 50°N 85°W	SAR images showed apparent circular feature ~180 km diameter	Cryovolcanic dome or shield (Elachi et al., 2005; Lopes et al., 2007); tectonic/erosional feature (Lopes et al., 2010)	No (new SAR data showing topography showed it is not a dome or shield)
Tortola Facula 9°N 143°W	VIMS image showed an apparent depression and lobate features ("snail-like")	Caldera and cryovolcanic flows (Sotin et al., 2005); hummocky and mountainous terrain (Lopes et al., 2010)	No (SAR data showed that VIMS apparent caldera and lobate features were superficial deposits only)
Hotei Regio 26°S 79°W	VIMS possible brightness changes, SAR images show lobate features	Cryovolcanic, active area (Nelson et al., 2009b); cryovolcanic flows (Wall et al., 2009; Soderblom et al., 2009); fluvial deposits (Moore and Howard, 2010)	Maybe (lobate flowlike features present in VIMS and SAR images; IR brightness changes contested by Soderblom et al. (2009)
Tui Regio 24°S 125°W	Flow like lobate features seen in VIMS data and later in SAR images	Cryovolcanic flows (Barnes et al., 2006); crater ejecta and unknown bright materials (Moore and Howard, 2010); lake bed with evaporate deposits (Barnes et al., 2011a)	Probably no (new analysis suggests lake bed)
Western Xanadu 10°S 140°W	Lobate overlapping features similar to Hotei and north Sotra	Cryovolcanic active area (Nelson et al., 2009a); cryovolcanic flows (Wall et al., 2009)	Maybe (lobate features seen in SAR, similar to those in Sotra northern region). IR brightness changes contested by Soderblom et al. (2009)
"T3 flow" 20°N 70°W	SAR and VIMS	Cryovolcanic flow (Lopes et al., 2007); (Le Corre et al., 2009)	Maybe (no new data available)
Rohe Fluctus 47°N 38°W	SAR	Caldera and cryovolcanic flow (Lopes et al., 2007)	Maybe (no new data available)
Ara Fluctus 40°N 118°W	SAR	Caldera and cryovolcanic flow (Lopes et al., 2007); coincidence of an impact crater and mottled materials (Moore and Howard, 2010)	Maybe (no new data available)
Winia Fluctus 45°N 30°W	SAR image shows large radar-bright lobate feature	Cryovolcanic flow field (Lopes et al., 2007); mass wasting or fluvial deposits (Moore and Howard, 2010)	Probably no (limited topography along SAR swath not consistent with elevated flow; (Lopes et al., 2011)
Sotra Facula 15°S 40°W	SAR image shows two mountains separated by lobate, flow-like features. One mountain is adjacent to a deep, non-circular pit	Southern feature interpreted as cryovolcanic (Lopes et al., 2010); combination of exogenic processes (Moore and Howard, 2010)	Probably yes – strongest candidates to date (Lopes et al., 2011)

cryomagma, reducing the distribution of explosive products, and would speed the cooling of cryolavas. According to Lorenz (1996), cryovolcanic eruptions on Titan, either present-day or in the past, are more likely effusive than explosive, as a result of both the high atmospheric pressure and the relatively volatile-poor magma compositions (<1% methane) that are predicted. This is consistent with candidate features such as flows; however, the Sotra pit described previously suggests explosive activity generating mountains and associated depressions. If cryoflows are indeed present on Titan, their composition is likely primarily

a mixture of water ice and ammonia, possibly with some methanol (Kargel, 1995; Kargel et al., 1991; Lorenz, 1996), although alternative compositions have been suggested, such as ammonium sulfates (Fortes and Grindrod, 2006). Ammonia-water-methanol compositions are expected to produce relatively high-viscosity, thick flows, consistent with measurements at Rohe Fluctus (Lopes et al., 2007) and Hotei (Kirk et al., 2012).

The mechanism of ascent of cryomagmas in icy satellites is still not fully understood. Ascent models have been based mostly on terrestrial models, proposing that cryomagmas rise due to thermal buoyancy from the mantle into the lower ice shell, potentially stalling close to the surface to form a cryomagma chamber, and then erupting through conduits formed by the intrusion of dikes. There are problems with this general mechanism, because the density of all proposed unvesiculated cryomagmas is greater than that of water-ice (specifically Ice-I, the inferred bulk composition of icy satellite crusts), so watery cryomagmas are negatively buoyant. As discussed by Lopes et al. (2012), a number of mechanisms have been proposed to overcome the negative buoyancy of cryomagma, such as inducing positive buoyancy through exsolution of volatiles following decompression and the subsequent ascent of fluid-filled fractures from the base of the ice shell (Crawford and Stevenson, 1988; Lorenz, 1996), or explosive eruption of sprays (Fagents et al., 2000). Other possible mechanisms include the pressurization of discrete liquid chambers (Fagents, 2003; Showman et al., 2004) or an entire ocean during freezing and volume changes (Manga and Wang, 2007), leading to effusive eruptions; partial melting of the ice shell by tidal dissipation (Mitri and Showman, 2008; Tobie et al., 2008); incorporation of denser silicate material in the ice shell (due to incomplete differentiation of meteoritic infall [Croft et al., 1988]); and solid state convection in the ice shell advecting heat and possibly chemicals upward and mobilizing near-surface pockets of salt- or ammonia-rich ices (Head et al., 1999; Mitri et al., 2008; Choukroun and Grasset, 2010). Despite direct observations of active eruptions at Enceladus, there is little direct evidence to support any of these mechanisms and the question of ascent of cryomagmas in icy crusts remains open.

2.11 Summary

The *Cassini-Huygens* mission to Titan has revealed a world that experiences surface temperatures 200 degrees colder than Earth's and receives 100 times less sunlight, where hydrocarbon molecules rain from the sky and water ice may be as hard as rock. But for all of its strange properties, Titan exhibits landforms remarkably familiar to our own: extensive dunes in dry regions, fluvial valley networks draining from mountains to large basins, and, perhaps most astonishingly, large liquid-filled seas and lakes. The associated processes are likewise analogous to those on Earth, including aeolian, pluvial, fluvial, lacustrine, tectonic, and impact processes, as well as putative cryovolcanic eruptions and long-term climate cycles.

Acknowledgments

The authors wish to thank two careful reviewers, helpful discussions with L. Soderblom, J. Barnes, and others, and the talented *Cassini-Huygens* engineering teams, without whom this research would not have been possible. Part of this work was conducted at the Jet Propulsion Laboratory, under contract with NASA.

References

Aharonson, O., Hayes, A. G., Lunine, J. I., Lorenz, R. D., et al. 2009. An asymmetric distribution of lakes on Titan as a possible consequence of orbital forcing. *Nature Geosciences*, **2**, 851–854. doi: 10.1038/ngeo698.

Artemieva, N., and Lunine, J. I. 2005. Impact cratering on Titan II. Global melt, escaping ejecta, and aqueous alteration of surface organics. *Icarus*, **175**, 522–533. doi: 10.1016/j.icarus.2004.12.005.

Atreya, S. K., Adams, E. Y., Niemann, H. B., Demick-Montelara, J. E., et al. 2006. Titan's methane cycle. *Planet. Space Sci.*, **54**, 1177–1187. doi: 10.1016/j.pss.2006.05.028.

Barnes, J. W., Brown, R. H., Turtle, E. P., McEwen, A. S., et al. 2005. A 5-micron-bright spot on Titan: evidence for surface diversity. *Science*, **310**, 92–95. doi: 10.1126/science.1117075.

Barnes, J. W., Brown, R. H., Radebaugh, J., Buratti, B. J., et al. 2006. Cassini observations of flow-like features in western Tui Regio, Titan. *Geophys. Res. Lett.*, **33**, 16204. doi: 10.1029/2006GL026843.

Barnes, J. W., Radebaugh, J., Brown, R. H., Wall, S., et al. 2007. Near-infrared spectral mapping of Titan's mountains and channels. *J. Geophys. Res.*, **112**(E11), 11006. doi: 10.1029/2007JE002932.

Barnes, J. W., Brown, R. H., Soderblom, L., Sotin, C., et al. 2008. Spectroscopy, morphometry, and photoclinometry of Titan's dunefields from Cassini/VIMS. *Icarus*, **195**, 400–414. doi: 10.1016/j.icarus.2007.12.006.

Barnes, J. W., Brown, R. H., Soderblom, J. M., Soderblom, L. A., et al. 2009a. Shoreline features of Titan's Ontario Lacus from Cassini/VIMS observations. *Icarus*, **201**, 217–225. doi: 10.1016/j.icarus.2008.12.028.

Barnes, J. W., Soderblom, J. M., Brown, R. H., Buratti, B. J., et al. 2009b. VIMS spectral mapping observations of Titan during the Cassini prime mission. *Planet. Spac. Sci*, **57**, 1950–1962. doi: 10.1016/j.pss.2009.04.013.

Barnes, J. W., Bow, J., Schwartz, J., Brown, R. H., et al. 2011a. Organic sedimentary deposits in Titan's dry lakebeds: Probable evaporite. *Icarus*, **216**, 136–140. doi: 10.1016/j.icarus.2011.08.022.

Barnes, J. W., Soderblom, J. M., Brown, R. H., Soderblom, L. A., et al. 2011b. Wave constraints for Titan's Jingpo Lacus and Kraken Mare from VIMS specular reflection lightcurves. *Icarus*, **211**, 722–731. doi: 10.1016/j.icarus.2010.09.022.

Black, B. A., Perron, J. T., Drummond, S., and Burr, D. M. 2012. Estimating erosional exhumation on Titan from drainage network morphology. *J. Geophys. Res.*, **117**, E08006, doi: 10.1029/2012JE00405.

Black, G. J., Campbell, D. B., and Carter, L. M. 2011. Ground-based radar observations of Titan: 2000–2008. *Icarus*, **212**, 300–320. doi: 10.1016/j.icarus.2010.10.025.

Black, Thomas A., and Montgomery, David R. 1991. Sediment transport by burrowing mammals, Marin County, California. *Earth Surface Processes and Landforms*, **16**(2), 163–172.

Bourgeois, O., Lopez, T., Le Mouélic, S, Fleurant, C., et al. 2008. A surface dissolution/precipitation model for the development of lakes on Titan, based on an arid terrestrial analogue: the pans and calcretes of Etosha (Namibia). Page 1733 of *Lunar and Planetary Institute Science Conference Abstracts*.

Brown, M. E., Schaller, E. L., Roe, H. G., Chen, C., et al. 2009. Discovery of lake-effect clouds on Titan. *Geophy. Res. Lett.*, **36**, L1103–L1108. doi: 10.1029/2008GL035964.

Brown, R. H., Baines, K. H., Bellucci, G., Bibring, J.-P., et al. 2004. The Cassini Visual and Infrared Mapping Spectrometer (VIMS) Investigation. *Spac. Sci. Rev.*, **115**, 111–168. doi: 10.1007/s11214-004-1453-x.

Brown, R. H., Soderblom, L. A., Soderblom, J. M., Clark, R. N., et al. 2008. The identification of liquid ethane in Titan's Ontario Lacus. *Nature*, **454**, 607–610. doi: 10.1038/nature07100.

Brown, R. H., Barnes, J. W., and Melosh, H. J. 2011. On Titan's Xanadu region. *Icarus*, **214**, 556–560. doi: 10.1016/j.icarus.2011.03.018.

Buratti, B. J., Sotin, C., Lawrence, K., Brown, R. H., et al. 2012. A newly discovered impact crater in Titan's Senkyo: Cassini VIMS observations and comparison with other impact features. *Planet. Spac. Sci.*, **60**, 18–25. doi: 10.1016/j.pss.2011.05.004.

Burr, D. J., Perron, J. T., Lamb, M. P., Irwin, R. P., et al. 2013. Fluvial features on Titan: Insights from morphology and modeling. *GSA Bulletin*, in press, doi: 10.1130/B30612.1.

Burr, D. M., Emery, J. P., Lorenz, R. D., Collins, G. C., et al. 2006. Sediment transport by liquid surficial flow: Application to Titan. *Icarus*, **181**(1), 235–242.

Burr, D. M., Jacobsen, R. E, Roth, D. L, Phillips, C. B, et al. 2009. Fluvial network analysis on Titan: Evidence for subsurface structures and west-to-east wind flow, southwestern Xanadu. *Geophys. Res. Lett*, **36**(22), L22203–.

Campbell, D. B., Black, G. J., Carter, L. M., and Ostro, S. J. 2003. Radar evidence for liquid surfaces on Titan. *Science*, **302**, 431–434. doi: 10.1126/science.1088969.

Choukroun, M., and Grasset, O. 2010. Thermodynamic data and modeling of the water and ammonia-water phase diagrams up to 2.2 GPa for planetary geophysics. *J. Chem. Phys.*, **133**(14), 144502. doi: 10.1063/1.3487520.

Clark, R. N., Curchin, J. M., Barnes, J. W., Jaumann, R., et al. 2010. Detection and mapping of hydrocarbon deposits on Titan. *J. Geophys. Res.*, **115**(E14), E10005. doi: 10.1029/2009JE003369.

Collins, G. C. 2005. Relative rates of fluvial bedrock incision on Titan and Earth. *Geophys. Res. Lett*, **32**(22), L22202.

Cordier, D., Mousis, O., Lunine, J. I., Lavvas, P., et al. 2009. An estimate of the chemical composition of Titan's lakes. *Astrophys. J. Lett.*, **707**, L128–L131. doi: 10.1088/0004-637X/707/2/L128.

Cornet, T., Le Mouélic, S., Bourgeois, O., Rodriguez, S., et al. 2010. Observation of Ontario Lacus on Titan with Cassini/VIMS at 17 months interval. Page 1370 of *Lunar and Planetary Institute Science Conference Abstracts*. Lunar and Planetary Inst. Technical Report, vol. 41.

Cornet, T., Bourgeois, O., Le Mouélic, S., Rodriguez, S., et al. 2012. Geomorphological significance of Ontario Lacus on Titan: Integrated interpretation of Cassini VIMS, ISS and RADAR data and comparison with the Etosha Pan (Namibia). *Icarus*, **218**(Apr.), 788–806. doi: 10.1016/j.icarus.2012.01.013.

Coustenis, A., Lellouch, E., Maillard, J. P., and McKay, C. P. 1995. Titan's surface: composition and variability from the near-infrared albedo. *Icarus*, **118**, 87–104. doi: 10.1006/icar.1995.1179.

Coustenis, A., Negrão, A., Salama, A., Schulz, B., et al. 2006. Titan's 3-micron spectral region from ISO high-resolution spectroscopy. *Icarus*, **180**, 176–185. doi: 10.1016/j.icarus.2005.08.007.

Crawford, G. D., and Stevenson, D. J. 1988. Gas-driven water volcanism in the resurfacing of Europa. *Icarus*, **73**, 66–79. doi: 10.1016/0019-1035(88)90085-1.

Croft, S. K., Lunine, J. I., and Kargel, J. 1988. Equation of state of ammonia-water liquid – derivation and

planetological applications. *Icarus*, **73**, 279–293. doi: 10.1016/0019-1035(88)90098-X.

Deledalle, C.-A., Denis, L., and Tupin, F. 2009. Iterative weighted maximum likelihood denoising with probabilistic patch-based weights. *Image Processing, IEEE Transactions on*, **18**(12), 2661 –2672. doi: 10.1109/TIP.2009.2029593.

Dietrich, W. E, and Perron, J. T. 2006. The search for a topographic signature of life. *Nature*, **439**(7075), 411–418.

Dietrich, W. E, Bellugi, D. G., Sklar, L. S., Stock, J. D., et al. 2003. Geomorphic transport laws for predicting landscape form and dynamics. Pages 103–132 of Wilcock, P. R., and Iverson, R. M. (eds), *Prediction in Geomorphology*. Washington, DC: American Geophysical Union.

Donelan, M. A., and Pierson, W. J. 1987. Radar scattering and equilibrium ranges in wind-generated waves with application to scatterometry. *J. Geophys. Res.*, **92**, 4971–5030. doi: 10.1029/JC092iC05p04971.

Donelan, M. A., and Plant, W. J. 2009. A threshold for wind-wave growth. *J. Geophys. Res.*, **114**(C13), 7012. doi: 10.1029/2008JC005238.

Dunne, T. 1980. Formation and controls of channel networks. *Progress in Physical Geography*, **4**(2), 211.

Elachi, C., Im, E., Roth, L. E., and Werner, C. L. 1991. Cassini Titan Radar Mapper. *Proceedings of the IEEE*, **79**(6), 867 –880. doi: 10.1109/5.90164.

Elachi, C., Allison, M. D., Borgarelli, L., Encrenaz, P., et al. 2004. RADAR: The Cassini Titan Radar Mapper. *Spac. Sci. Rev.*, **115**, 71–110. doi: 10.1007/s11214-004-1438-9.

Elachi, C., Wall, S., Allison, M., Anderson, Y., et al. 2005. Cassini radar views the surface of Titan. *Science*, **308**, 970–974. doi: 10.1126/science.1109919.

Elachi, C., Wall, S., Janssen, M., Stofan, E., et al. 2006. Titan Radar Mapper observations from Cassini's T_3 fly-by. *Nature*, **441**, 709–713. doi: 10.1038/nature04786.

Fagents, S. A. 2003. Considerations for effusive cryovolcanism on Europa: The post-Galileo perspective. *J. Geophys. Res.*, **108**, 5139. doi: 10.1029/2003JE002128.

Fagents, S. A., Greeley, R., Sullivan, R. J., Pappalardo, R. T., et al. and the Galileo SSI Team. 2000. Cryomagmatic mechanisms for the formation of Rhadamanthys Linea, triple band margins, and other low-albedo features on Europa. *Icarus*, **144**, 54–88. doi: 10.1006/icar.1999.6254.

Fortes, A. D., and Grindrod, P. M. 2006. Modelling of possible mud volcanism on Titan. *Icarus*, **182**, 550–558. doi: 10.1016/j.icarus.2005.11.013.

Gabet, E. J, Reichman, O. J, and Seabloom, E. W. 2003. The effects of bioturbation on soil processes and sediment transport. *Annu. Rev. Earth Planet. Sci.*, **31**(1), 249–273.

Gehrels, T., Baker, L. R., Beshore, E., Blenman, C., et al. 1980. Imaging photopolarimeter on Pioneer Saturn. *Science*, **207**, 434–439. doi: 10.1126/science.207.4429.434.

Griffith, C. A., Owen, T., Geballe, T. R., Rayner, J., et al. 2003. Evidence for the exposure of water ice on Titan's surface. *Science*, **300**, 628–630. doi: 10.1126/science.1081897.

Gulick, V. C. 2001. Origin of the valley networks on Mars: a hydrological perspective. *Geomorphology*, **37**(3–4), 241–268.

Hanel, R., Conrath, B., Flasar, F. M., Kunde, V., et al. 1981. Infrared observations of the Saturnian system from Voyager 1. *Science*, **212**, 192–200. doi: 10.1126/science.212.4491.192.

Hayes, A. G., Aharonson, O., Callahan, P., Elachi, C., et al. 2008. Hydrocarbon lakes on Titan: Distribution and interaction with a porous regolith. *Geophys. Res. Lett.*, **35**, 9204–9208. doi: 10.1029/2008GL033409.

Hayes, A. G., Wolf, A. S., Aharonson, O., Zebker, H., et al. 2010. Bathymetry and absorptivity of Titan's Ontario Lacus. *J. Geophys. Res.*, **115**(E09009). doi: 10.1029/2009JE003557.

Hayes, A. G., Aharonson, O., Lunine, J. I., Kirk, R. L., et al. and the Cassini RADAR Team. 2011a. Transient surface liquid in Titan's polar regions from Cassini. *Icarus*, **211**. doi: 10.1016/j.icarus.2010.07.017.

Hayes, A. G., Lorenz, R. D., Donelan, M. A., Lamb, M. P., et al. and the Cassini RADAR Team. 2011b. Wind driven capillary-gravity waves on Titan's lakes: hard to detect or non-existent? *Icarus*, submitted.

Hayes, A. G., and Ewing, R. C. 2011. Reorientation timescales and pattern dynamics for titan's dunes: Does the tail wag the dog or the dragon? Pages P33F–01 of: *AGU Fall Meeting Abstracts*.

Head, J. W., Pappalardo, R. T., and Sullivan, R. 1999. Europa: Morphological characteristics of ridges and triple bands from Galileo data (E4 and E6) and assessment of a linear diapirism model. *J. Geophys. Res*, **104**, 24223–24236. doi: 10.1029/1998JE001011.

Howard, A. D. 1988. Groundwater sapping experiments and modeling. *Sapping features of the Colorado Plateau: a comparative planetary geology field guide*, National Aeronautics and Space Administration, Washington, DC, SP-491, pp. 71–83.

Hueso, R, and Sánchez-Lavega, A. 2006. Methane storms on Saturn's moon Titan. *Nature*, **442**(7101), 428–431.

Hunten, D. M. 1978. A Titan atmosphere with a surface temperature of 200K. Pages 127–140 of D. M. Hunten and D. Morrison (eds.), *NASA Conference Publication*. NASA Conference Publications, vol. 2068.

Iess, L., Rappaport, N. J., Jacobson, R. A., Racioppa, P., et al. 2010. Gravity field, shape, and moment of inertia of Titan. *Science*, **327**, 1367–1369. doi: 10.1126/science.1182583.

Ivanov, B. A., Basilevsky, A. T., and Neukum, G. 1997. Atmospheric entry of large meteoroids: implication to Titan. *Planet. Space Sci.*, **45**(8), 993–1007. doi: 10.1016/S0032-0633(97)00044-5.

Janssen, M. A., Lorenz, R. D., West, R., Paganelli, F., et al. and the Cassini Radar Team. 2009. Titan's surface at 2.2-cm wavelength imaged by the Cassini RADAR

radiometer: Calibration and first results. *Icarus*, **200**, 222–239. doi: 10.1016/j.icarus.2008.10.017.

Janssen, M. A., Le Gall, A. A., and Chaudhuri, S. 2010. Global mapping of Titan at 2-cm wavelength. *AGU Fall Meeting Abstracts*.

Janssen, M. A., Le Gall, A., and Wye, L. C. 2011. Anomalous radar backscatter from Titan's surface? *Icarus*, **212**, 321–328. doi: 10.1016/j.icarus.2010.11.026.

Jaumann, R., Brown, R. H., Stephan, K., Barnes, J. W., et al. 2008. Fluvial erosion and post-erosional processes on Titan. *Icarus*, **197**(2), 526–538.

Jaumann, R., Kirk, R. L., Lorenz, R. D., Lopes, R. M. C., et al. 2009a. Geology and surface processes on Titan. Pages 75–140 of Brown, R. H., Lebreton, J.-P., and Waite, J. H. (eds.), *Titan from Cassini-Huygens*. Springer. doi: 10.1007/978-1-4020-9215-2_5.

Jaumann, R., Clark, R. N., Nimmo, F., Hendrix, A. R., et al. 2009b. Icy satellites: Geological evolution and surface processes. Pages 637–682 of Dougherty, M. K., Esposito, L. W., and Krimigis, S. M. (eds.), *Saturn from Cassini-Huygens*. Springer. doi: 10.1007/978-1-4020-9217-6_20.

Kargel, J. S. 1995. Cryovolcanism on the icy satellites. *Earth Moon and Planets*, **67**, 101–113.

Kargel, J. S., Croft, S. K., Lunine, J. I., and Lewis, J. S. 1991. Rheological properties of ammonia-water liquids and crystal-liquid slurries – planetological applications. *Icarus*, **89**, 93–112. doi: 10.1016/0019-1035(91)90090-G.

Kirk, R. L., Howington-Kraus, E., Redding, B. L., Becker, T. L., et al. and the Cassini Radar Team. 2007. First stereoscopic radar images of Titan. Page 1427 of: *Lunar and Planetary Institute Conference Abstracts*. Lunar and Planetary Institute Conference Abstracts, vol. 38.

Kirk, R. L., Howington-Kraus, E., Barnes, J. W., Hayes, A. G., et al. 2010. La Sotra y las otras: Topographic evidence for (and against) cryovolcanism on Titan (Invited). *AGU Fall Meeting Abstracts*, A3.

Kirk, R. L., Howington-Kraus, E., Redding, B. L., Becker, T. L., et al. and the Cassini Radar Team. 2012. High resolution topographic models of Titan's surface derived by radar stereogrammetry with a rigorous sensor model. *Icarus*, in revision.

Kirk, R. L., Wood, C. A., Neish, C., Lucas, A., et al. 2011. Morphometry and morphology of fresh craters on Titan. Pages P32C–08 of *AGU Fall Meeting Abstracts*.

Korycansky, D. G., and Zahnle, K. J. 2005. Modeling crater populations on Venus and Titan. *Planet. Space Sci.*, **53**, 695–710. doi: 10.1016/j.pss.2005.03.002.

Kuiper, G. P. 1944. Titan: a satellite with an atmosphere. *Astrophys. J.*, **100**. doi: 10.1086/144679.

Lamb, M. P., Howard, A. D., Dietrich, W. E., and Perron, J. T. 2007. Formation of amphitheater-headed valleys by waterfall erosion after large-scale slumping on Hawai'i. *Geological Society of America Bulletin*, **119**(7–8), 805–822.

Lamb, M. P., Howard, A. D., Johnson, J., Whipple, K. X., et al. 2006. Can springs cut canyons into rock? *J. Geophys. Res.*, **111**(E7), E07002.

Lamb, M. P., Dietrich, W. E., Aciego, S. M., DePaolo, D. J., et al. 2008. Formation of Box Canyon, Idaho, by megaflood: Implications for seepage erosion on Earth and Mars. *Science*, **320**(5879), 1067.

Langhans, M. H., Jaumann, R., Stephan, K., Brown, R. H., et al. 2011. Titan's fluvial valleys: Morphology, distribution, and spectral properties. *Planet. Spac. Sci.*

Larsen, I. J., Montgomery, D. R., and Korup, O. 2010. Landslide erosion controlled by hillslope material. *Nature Geoscience*, **3**(4), 247–251.

Le Corre, L., Le Mouélic, S., Sotin, C., Combe, J.-P., et al. 2009. Analysis of a cryolava flow-like feature on Titan. *Planet. Space Sci.*, **57**, 870–879. doi: 10.1016/j.pss.2009.03.005.

Le Gall, A., Janssen, M. A., Paillou, P., Lorenz, R. D., et al. 2010. Radar-bright channels on Titan. *Icarus*, **207**(2), 948–958.

Le Gall, A., Janssen, M. A., Wye, L. C., Hayes, A. G., et al. and the Cassini Radar Team. 2011. Cassini SAR, radiometry, scatterometry and altimetry observations of Titan's dune fields. *Icarus*, **213**, 608–624. doi: 10.1016/j.icarus.2011.03.026.

Lindal, G. F., Wood, G. E., Hotz, H. B., Sweetnam, D. N., et al. 1983. The atmosphere of Titan – an analysis of the Voyager 1 radio occultation measurements. *Icarus*, **53**, 348–363. doi: 10.1016/0019-1035(83)90155-0.

Litwin, K. L., Polito, P., Zygielbaum, B., Sklar, L. S., et al. 2010. The influence of impurities in Titan ice bedrock on tensile strength and resistance to fluvial erosion: experimental results. Pages P31C–1554 of *AGU Fall Meeting Abstracts*.

Lopes, R. M. C., Mitchell, K. L., Stofan, E. R., Lunine, J. I., et al. 2007. Cryovolcanic features on Titan's surface as revealed by the Cassini Titan Radar Mapper. *Icarus*, **186**, 395–412. doi: 10.1016/j.icarus.2006.09.006.

Lopes, R. M. C., Stofan, E. R., Peckyno, R., Radebaugh, J., et al. and the Cassini RADAR Team. 2010. Distribution and interplay of geologic processes on Titan from Cassini radar data. *Icarus*, **205**, 540–558. doi: 10.1016/j.icarus.2009.08.010.

Lopes, R. M. C., Kirk, R., Mitchell, K. L., LeGall, A., et al. 2011. Cryovolcanism on Titan: new results from Cassini RADAR and VIMS. *Icarus*, submitted.

Lopes, R. M. C., Fagents, S. A., Mitchell, K. L., and Gregg, T. K. P. 2012. Planetary volcanism. In: Fagents, S. A., Gregg, T. K. P., and Lopes, R. M. C. (eds.), *Modelling Volcanic Processes*. Cambridge University Press.

Lorenz, R. D. 1996. Pillow lava on Titan: expectations and constraints on cryovolcanic processes. *Planet. Spac. Sci.*, **44**, 1021–1028. doi: 10.1016/0032-0633(95)00139-5.

Lorenz, R. D., and Lunine, J. I. 1996. Erosion on Titan: past and present. *Icarus*, **122**, 79–91. doi: 10.1006/icar.1996.0110.

Lorenz, R. D., and Radebaugh, J. 2009. Global pattern of Titan's dunes: Radar survey from the Cassini prime

mission. *Geophys. Res. Lett.*, **360**, L03202. doi: 10.1029/2008GL036850.

Lorenz, R. D., Wall, S., Radebaugh, J., Boubin, G., et al. 2006a. The sand seas of Titan: Cassini RADAR Observations of longitudinal dunes. *Science*, **312**, 724–727. doi: 10.1126/science.1123257.

Lorenz, R. D., Niemann, H. B., Harpold, D. N., Way, S. H., et al. 2006b. Titan's damp ground: Constraints on Titan surface thermal properties from the temperature evolution of the Huygens GCMS inlet. *Meteoritics and Planetary Science*, **41**, 1705–1714.

Lorenz, R. D., Mitchell, K. L., Kirk, R. L., Hayes, A. G., et al. 2008a. Titan's inventory of organic surface materials. *Geophys. Res. Lett.*, **35**, 2206. doi: 10.1029/2007GL032118.

Lorenz, R. D., Mitchell, K. L., Kirk, R. L., Hayes, A. G. et al., 2008b. Titan's inventory of organic surface materials. *Geophysical Research Letters*, **35**, L2206:1–6. doi: 10.1029/2007GL032118.

Lorenz, R. D., Newman, C., and Lunine, J. I. 2010. Threshold of wave generation on Titan's lakes and seas: Effect of viscosity and implications for Cassini observations. *Icarus*, **207**, 932–937. doi: 10.1016/j.icarus.2009.12.004.

Lorenz, R. D., Tokano, T., and Newman, C. E. in press. Wind and tides of Ligeia Mare: Application to the drift of the Titan Mare Explorer (TiME) mission. *Planet. Space Sci.*

Lorenz, R. D., and Lunine, J. I. 1996. Erosion on Titan: Past and present. *Icarus*, **122**(1), 79–91.

Lorenz, R. D., Lopes, R. M., Paganelli, F., Lunine, J. I., et al. 2008. Fluvial channels on Titan: initial Cassini RADAR observations. *Planet. Space Sci.*, **56**(8), 1132–1144.

Lucas, A., Aharonson, O., Hayes, A. G., Deledalle, C. A., et al. 2011. Enhanced processing and analysis of Cassini SAR images of Titan. *AGU Fall Meeting Suppl.*, P33E–1795.

Lunine, J. I., Stevenson, D. J., and Yung, Y. L. 1983. Ethane ocean on Titan. *Science*, **222**, 1229–+. doi: 10.1126/science.222.4629.1229.

Lunine, J. I., Elachi, C, Wall, S. D., Janssen, M. A., et al. 2008. Titan's diverse landscapes as evidenced by Cassini RADAR's third and fourth looks at Titan. *Icarus*, **195**(1), 415–433.

Malaska, M., Radebaugh, J., Lorenz, R., Mitchell, K., et al. 2010. Identification of Karst-like terrain on Titan from valley analysis. Page 1544 of: *Lunar and Planetary Institute Science Conference Abstracts*. Lunar and Planetary Inst. Technical Report, vol. 41.

Malin, M. C., and Carr, M. H. 1999. Groundwater formation of martian valleys. *Nature*, **397**(6720), 589–591.

Manga, M., and Wang, C.-Y. 2007. Pressurized oceans and the eruption of liquid water on Europa and Enceladus. *Geophys. Res. Lett.*, **34**, 7202. doi: 10.1029/2007GL029297.

McCord, T. B., Hansen, G. B., Buratti, B. J., Clark, R. N., et al. and the Cassini VIMS Team. 2006. Composition of Titan's surface from Cassini VIMS. *Planet. Spac. Sci.*, **54**, 1524–1539. doi: 10.1016/j.pss.2006.06.007.

McCord, T. B., Hayne, P., Combe, J.-P., Hansen, G. B., et al. and the Cassini VIMS Team. 2008. Titan's surface: Search for spectral diversity and composition using the Cassini VIMS investigation. *Icarus*, **194**, 212–242. doi: 10.1016/j.icarus.2007.08.039.

Mitchell, J. L. 2008. The drying of Titan's dunes: Titan's methane hydrology and its impact on atmospheric circulation. *J. Geophys. Res. Planets*, **113**(E12), E8015:1–22. doi: 10.1029/2007JE003017.

Mitchell, K. L., Kargel, J. S., Wood, C. A., Radebaugh, J. et al.and Cassini Radar Team. 2007. Titan's crater lakes: Caldera vs. Karst. Page 2064 of *Lunar and Planetary Institute Science Conference Abstracts*. Lunar and Planetary Inst. Technical Report, vol. 38.

Mitchell, K. L., Stiles, B., Zebker, H. A., Kirk, R. L., et al. and Cassini Radar Team. 2009. A global subsurface alkanofer system on Titan? Page 1966 of *Lunar and Planetary Institute Science Conference Abstracts*. Lunar and Planetary Inst. Technical Report, vol. 40.

Mitri, G., and Showman, A. P. 2008. Thermal convection in ice-I shells of Titan and Enceladus. *Icarus*, **193**, 387–396. doi: 10.1016/j.icarus.2007.07.016.

Mitri, G., Showman, A. P., Lunine, J. I., and Lorenz, R. D. 2007. Hydrocarbon lakes on Titan. *Icarus*, **186**, 385–394. doi: 10.1016/j.icarus.2006.09.004.

Mitri, G., Showman, A. P., Lunine, J. I., and Lopes, R. M. C. 2008. Resurfacing of Titan by ammonia-water cryomagma. *Icarus*, **196**, 216–224. doi: 10.1016/j.icarus.2008.02.024.

Mitri, G., Bland, M. T., Showman, A. P., Radebaugh, J., et al. 2010. Mountains on Titan: Modeling and observations. *J. Geophys. Res.*, **115**(E14), E10002. doi: 10.1029/2010JE003592.

Montgomery, D. R., and Brandon, M. T. 2002. Topographic controls on erosion rates in tectonically active mountain ranges. *Earth and Planetary Science Letters*, **201**(3–4), 481–489.

Moore, J. M., and Howard, A. D. 2010. Are the basins of Titan's Hotei Regio and Tui Regio sites of former low latitude seas? *Geophys. Res. Lett.*, **37**, 22205. doi: 10.1029/2010GL045234.

Moore, J. M., and Pappalardo, R. T. 2011. Titan: An exogenic world? *Icarus*, **212**, 790–806. doi: 10.1016/j.icarus.2011.01.019.

Neish, C. D., and Lorenz, R. D. 2012. Titan's global crater population: A new assessment. *Planet. Space Sci.*, **60**(Jan.), 26–33. doi: 10.1016/j.pss.2011.02.016.

Neish, C. D., Lorenz, R. D., Kirk, R. L., and Wye, L. C. 2010. Radarclinometry of the sand seas of Africa's Namibia and Saturn's moon Titan. *Icarus*, **208**, 385–394. doi: 10.1016/j.icarus.2010.01.023.

Nelson, R. M., Kamp, L. W., Lopes, R. M. C., Matson, D. L., et al. 2009a. Photometric changes on Saturn's Titan: Evidence for active cryovolcanism. *Geophys. Res. Lett.*, **36**, 4202. doi: 10.1029/2008GL036206.

Nelson, R. M., Kamp, L. W., Matson, D. L., Irwin, P. G. J., et al. 2009b. Saturn's Titan: Surface change, ammonia, and implications for atmospheric and tectonic

activity. *Icarus*, **199**, 429–441. doi: 10.1016/j.icarus.2008.08.013.

Niemann, H. B., Atreya, S. K., Bauer, S. J., Biemann, K., et al. 2002. The Gas Chromatograph Mass Spectrometer for the Huygens Probe. *Space. Sci. Rev.*, **104**, 553–591. doi: 10.1023/A:1023680305259.

Niemann, H. B., Atreya, S. K., Demick, J. E., Gautier, D. et al. 2010. Composition of Titan's lower atmosphere and simple surface volatiles as measured by the Cassini-Huygens probe gas chromatograph mass spectrometer experiment. *J. Geophys. Res.*, **115**(E14), 12006. doi: 10.1029/2010JE003659.

Notarnicola, C., Ventura, B., Casarano, D., and Posa, F. 2009. Cassini radar data: Estimation of Titan's lake features by means of a Bayesian inversion algorithm. *Geoscience and Remote Sensing, IEEE Transactions on*, **47**(5), 1503–1511. doi: 10.1109/TGRS.2008.2005906.

Paganelli, F., Janssen, M. A., Stiles, B., West, R., et al. and the Radar Team. 2007. Titan's surface from Cassini RADAR SAR and high resolution radiometry data of the first five flybys. *Icarus*, **191**, 211–222. doi: 10.1016/j.icarus.2007.04.032.

Paillou, P., Mitchell, K., Wall, S., Ruffié, G., et al. 2008a. Microwave dielectric constant of liquid hydrocarbons: Application to the depth estimation of Titan's lakes. *Geophysical Research Letters*, **35**, L05202:1–5. doi: 10.1029/2007GL032515.

Paillou, P., Lunine, J., Ruffié, G., Encrenaz, P., et al. 2008b. Microwave dielectric constant of Titan-relevant materials. *Geophys. Res. Lett.*, **35**, 18202. doi: 10.1029/2008GL035216.

Parker, G. 2005. Comparative Application of Dimensionless bankfull hydraulic relations for Earth and Titan. Pages H31G–06 of *AGU Fall Meeting Abstracts*.

Parker, Gary. 1975. Meandering of supraglacial melt streams. *Water Resour. Res*, **11**(4), 551–552.

Perron, J. T., and de Pater, I. 2004. Dynamics of an ice continent on Titan. *Geophys. Res. Lett*, **31**(17), L17S04–. doi: 10.1029/2004GL019802.

Perron, J. T., and Fagherazzi, S. 2012. The legacy of initial conditions in landscape evolution. *Earth Surface Processes and Landforms*, **37**(1), 52–63.

Perron, J. T., and Hamon, J. L. 2012. Equilibrium form of horizontally retreating, soil-mantled hillslopes: Model development and application to a groundwater sapping landscape. *J. Geophys. Res. (Earth Surface)*, **117**(F16), 1027. doi: 10.1029/2011JF002139.

Perron, J. T., Dietrich, W. E., Howard, A. D., McKean, J. A. et al. 2003. Ice-driven creep on Martian debris slopes. *Geophys. Res. Lett.*, **30**(14), 1747. doi: 10.1029/2003GL017603.

Perron, J. T., Lamb, M. P., Koven, C. D., Fung, I. Y., et al. 2006. Valley formation and methane precipitation rates on Titan. *J Geophys Res*, **111**, E11001. doi: 10.1029/2005JE002602.

Plant, W. J. 1982. A relationship between wind stress and wave slope. *J. Geophys. Res*, **87**, 1961–1967. doi: 10.1029/JC087iC03p01961.

Polito, P. J., Zygielbaum, B. R., Sklar, L. S., and Collins, G. 2008. Experimental investigation of fluvial incision on Titan by low-velocity sediment impacts. Pages P21A–1316 of *AGU Fall Meeting Abstracts*.

Porco, C. C., West, R. A., Squyres, S., McEwen, A., et al. 2004. Cassini imaging science: Instrument characteristics and anticipated scientific investigations at Saturn. *Spac. Sci. Rev.*, **115**, 363–497. doi: 10.1007/s11214-004-1456-7.

Porco, C. C., Baker, E., Barbara, J., Beurle, K., et al. 2005. Imaging of Titan from the Cassini spacecraft. *Nature*, **434**, 159–168. doi: 10.1038/nature03436.

Radebaugh, J., Lorenz, R. D., Kirk, R. L., Lunine, J. I., et al. and the Cassini RADAR Team. 2007. Mountains on Titan observed by Cassini Radar. *Icarus*, **192**, 77–91. doi: 10.1016/j.icarus.2007.06.020.

Radebaugh, J., Lorenz, R. D., Lunine, J. I., Wall, S. D., et al. and the Cassini Radar Team. 2008. Dunes on Titan observed by Cassini Radar. *Icarus*, **194**, 690–703. doi: 10.1016/j.icarus.2007.10.015.

Radebaugh, J., Baker, V., Lorenz, R. D., Farr, T. G., et al. and the Cassini RADAR Team. 2009. Fluvial erosion on Titan: Scales and landform modification. Page 36.07 of: *AAS/Division for Planetary Sciences Meeting Abstracts #41*. AAS/Division for Planetary Sciences Meeting Abstracts, vol. 41.

Radebaugh, J., Lorenz, R., Farr, T., Paillou, P., et al. 2010. Linear dunes on Titan and earth: Initial remote sensing comparisons. *Geomorphology*, **121**, 122–132. doi: 10.1016/j.geomorph.2009.02.022.

Radebaugh, J., Lorenz, R. D., Wall, S. D., Kirk, R. L., et al. and the Cassini Radar Team. 2011. Regional geomorphology and history of Titan's Xanadu province. *Icarus*, **211**, 672–685. doi: 10.1016/j.icarus.2010.07.022.

Radebaugh, J., Lorenz, R. D., Kirk, R. L., Lunine, J. I., et al. 2007. Mountains on Titan observed by Cassini Radar. *Icarus*, **192**(1), 77–91.

Richardson, J., Lorenz, R. D., and McEwen, A. 2004. Titan's surface and rotation: new results from Voyager 1 images. *Icarus*, **170**(1), 113–124. doi: 10.1016/j.icarus.2004.03.010.

Rubin, D. M., and Hesp, P. A. 2009. Multiple origins of linear dunes on Earth and Titan. *Nature Geoscience*, **2**, 653–658. doi: 10.1038/ngeo610.

Sagan, C., and Dermott, S. F. 1982. The tide in the seas of Titan. *Nature*, **300**, 731–733. doi: 10.1038/300731a0.

Schaller, E. L., Roe, H. G., Schneider, T., and Brown, M. E. 2009. Storms in the tropics of Titan. *Nature*, **460**, 873–875. doi: 10.1038/nature08193.

Schmidt, K. M., and Montgomery, D. R. 1995. Limits to relief. *Science*, **270**(5236), 617–620.

Schneider, T., Graves, S. D. B., Schaller, E. L., and Brown, M. E. 2012. Polar methane accumulation and rainstorms on Titan from simulations of the methane cycle. *Nature*, **481**, 58–61. doi: 10.1038/nature10666.

Schumm, S. A., Boyd, K. F., Wolff, C. G., and Spitz, W. J. 1995. A ground-water sapping landscape in the Florida Panhandle. *Geomorphology*, **12**(4), 281–297.

Sen, A. D., Anicich, V. G., and Arakelian, T. 1992. Dielectric constant of liquid alkanes and hydrocarbon mixtures. *J. Appl., Physics*, **25**, 512–521.

Showman, A. P., Mosqueira, I., and Head, J. W. 2004. On the resurfacing of Ganymede by liquid water volcanism. *Icarus*, **172**, 625–640. doi: 10.1016/j.icarus.2004.07.011.

Smith, P. H., Lemmon, M. T., Lorenz, R. D., Sromovsky, L. A., et al. 1996. Titan's surface, revealed by HST Imaging. *Icarus*, **119**, 336–349. doi: 10.1006/icar.1996.0023.

Soderblom, J. M., Brown, R. H., Soderblom, L. A., Barnes, J. W., et al. 2010. Geology of the Selk crater region on Titan from Cassini VIMS observations. *Icarus*, **208**, 905–912. doi: 10.1016/j.icarus.2010.03.001.

Soderblom, L., Brown, R. H., Soderblom, J. M., Barnes, J. W., et al. 2012. Composition and comparison of Titan's north and south polar lakes from Cassini visual and infrared mapping spectrometer observations. *Icarus*, submitted.

Soderblom, L. A., Kirk, R. L., Lunine, J. I., Anderson, J. A., et al. 2007. Correlations between Cassini VIMS spectra and RADAR SAR images: Implications for Titan's surface composition and the character of the Huygens Probe Landing Site. *Planet. Space Sci.*, **55**, 2025–2036. doi: 10.1016/j.pss.2007.04.014.

Soderblom, L. A., Brown, R. H., Soderblom, J. M., Barnes, J. W., et al. 2009. The geology of Hotei Regio, Titan: Correlation of Cassini VIMS and RADAR. *Icarus*, **204**, 610–618. doi: 10.1016/j.icarus.2009.07.033.

Soderblom, L. A., Tomasko, M. G., Archinal, B. A., Becker, T. L., et al. 2007. Topography and geomorphology of the Huygens landing site on Titan. *Planet. Space Sci.*, **55**(13), 2015–2024.

Sola, J. C. 1904. La sincérité scientifique. *Annals of the Observatory of Lucien Libert*, **18**, 51–53.

Sotin, C., Jaumann, R., Buratti, B. J., Brown, R. H., et al. 2005. Release of volatiles from a possible cryovolcano from near-infrared imaging of Titan. *Nature*, **435**, 786–789. doi: 10.1038/nature03596.

Sotin, C., Lawrence, K. J., Reinhardt, B., Barnes, J. W., et al. 2011. Observations of Titan's northern lakes at 5 microns: Implications for the organic cycle and geology. *Icarus*, submitted.

Stephan, K., Jaumann, R., Brown, R. H., Soderblom, J. M., et al. 2010. Specular reflection on Titan: Liquids in Kraken Mare. *Geophys. Res. Lett.*, **37**, L07104. doi: 10.1029/2009GL042312.

Stiles, B. W., Hensley, S., Gim, Y., Bates, D. M., et al. and the Cassini RADAR Team. 2009. Determining Titan surface topography from Cassini SAR data. *Icarus*, **202**, 584–598. doi: 10.1016/j.icarus.2009.03.032.

Stofan, E. R., Lunine, J. I., Lopes, R., Paganelli, F., et al. 2006. Mapping of Titan: Results from the first Titan radar passes. *Icarus*, **185**, 443–456. doi: 10.1016/j.icarus.2006.07.015.

Stofan, E. R., Elachi, C., Lunine, J. I., Lorenz, R. D., et al. 2007. The lakes of Titan. *Nature*, **445**, 61–64. doi: 10.1038/nature05438.

Stofan, E. R., Elachi, C., Lunine, J. I., Lorenz, R. D., et al. and the Cassini Radar Team. 2008. Varied geologic terrains at Titan's south pole: First results from T39. Page 1491 of *Lunar and Planetary Institute Science Conference Abstracts*. Lunar and Planetary Institute Science Conference Abstracts, vol. 39.

Tobie, G., Čadek, O., and Sotin, C. 2008. Solid tidal friction above a liquid water reservoir as the origin of the south pole hotspot on Enceladus. *Icarus*, **196**, 642–652. doi: 10.1016/j.icarus.2008.03.008.

Tokano, T. 2008. Dune-forming winds on Titan and the influence of topography. *Icarus*, **194**, 243–262. doi: 10.1016/j.icarus.2007.10.007.

Tokano, T. 2010. Relevance of fast westerlies at equinox for the eastward elongation of Titan's dunes. *Aeolian Research*, **2**, 113–127.

Tomasko, M. G., Buchhauser, D., Bushroe, M., Dafoe, L. E., et al. 2002. The Descent Imager/Spectral Radiometer (DISR) Experiment on the Huygens Entry Probe of Titan. *Spac. Sci. Rev.*, **104**, 469–551. doi: 10.1023/A:1023632422098.

Tomasko, M. G., Archinal, B., Becker, T., Bézard, B., et al. 2005. Rain, winds and haze during the Huygens probe's descent to Titan's surface. *Nature*, **438**(7069), 765–778.

Turtle, E. P., Perry, J. E., McEwen, A. S., DelGenio, A. D., et al. 2009. Cassini imaging of Titan's high-latitude lakes, clouds, and south-polar surface changes. *Geophys. Res. Lett.*, **36**, L2204:1–6. doi: 10.1029/2008GL036186.

Turtle, E. P., Perry, J. E., Hayes, A. G., Lorenz, R. D., et al. 2011a. Rapid and extensive surface changes near Titan's equator: Evidence of April showers. *Science*, **331**, 1414–. doi: 10.1126/science.1201063.

Turtle, E. P., Perry, J. E., Hayes, A. G., and McEwen, A. S. 2011b. Shoreline retreat at Titan's Ontario Lacus and Arrakis Planitia from Cassini Imaging Science Subsystem observations. *Icarus*, **212**, 957–959. doi: 10.1016/j.icarus.2011.02.005.

Wall, S., Hayes, A., Bristow, C., Lorenz, R., et al. 2010. Active shoreline of Ontario Lacus, Titan: A morphological study of the lake and its surroundings. *Geophys. Res. Lett.*, **37**, L5202:1–5. doi: 10.1029/2009GL041821.

Wall, S. D., Lopes, R. M., Stofan, E. R., Wood, C. A. et.al.2009. Cassini RADAR images at Hotei Arcus and western Xanadu, Titan: Evidence for geologically recent cryovolcanic activity. *Geophys. Res. Lett.*, **36**, 4203. doi: 10.1029/2008GL036415.

Warren, S. G., and Brandt, R. E. 2008. Optical constants of ice from the ultraviolet to the microwave: A revised compilation. *J. Geophys. Res.*, **113**, D14220. doi: 10.1029/2007JD009744.

Werner, B. T., and Kocurek, G. 1997. Bed-form dynamics: Does the tail wag the dog? *Geology*, **25**, 771. doi: 10.1130/0091-7613(1997)025!0771: BFDDTT¿2.3.CO;2.

West, R. A., and Smith, P. H. 1991. Evidence for aggregate particles in the atmospheres of Titan and Jupiter. *Icarus*, **90**, 330–333. doi: 10.1016/0019-1035(91)90113-8.

Wiscombe, W. J., and Warren, S. G. 1980. A model for the spectral albedo of snow. I: Pure snow. *J. Atmos. Sci.*, **37**(12), 2712–2733.

Wood, C. A., Mitchell, K. L., Lopes, R. M. C., Radebaugh, J., et al. 2007. Volcanic calderas in the north polar region of Titan. Pages 1454–+ of: *Lunar and Planetary Institute Science Conference Abstracts*. Lunar and Planetary Institute Science Conference Abstracts, vol. 38.

Wood, C. A., Lorenz, R., Kirk, R., Lopes, R., et al. 2010. Impact craters on Titan. *Icarus*, **206**(1), 334–344. doi: 10.1016/j.icarus.2009.08.021.

Wye, L., Zebker, H. A., Hayes, A. G., and Lorenz, R. D. 2010. A depth profile of titan's Ontario Lacus and further constraints on wave heights from Cassini RADAR data. Page 1076 of: *AAS/Division for Planetary Sciences Meeting Abstracts #42*, vol. 42.

Wye, L. C., Zebker, H. A., Ostro, S. J., West, R. D., et al. and the Cassini Radar Team. 2007. Electrical properties of Titan's surface from Cassini RADAR scatterometer measurements. *Icarus*, **188**, 367–385. doi: 10.1016/j.icarus.2006.12.008.

Wye, L. C., Zebker, H. A., and Lorenz, R. D. 2009. Smoothness of Titan's Ontario Lacus: Constraints from Cassini RADAR specular reflection data. *Geophys. Res. Lett.*, **36**, L16201:1–5. doi: 10.1029/2009GL039588.

Yung, Y. L., Allen, M., and Pinto, J. P. 1984. Photochemistry of the atmosphere of Titan – Comparison between model and observations. *Astrophys. J.*, **55**, 465–506. doi: 10.1086/190963.

Zarnecki, J. C., Leese, M. R., Hathi, B., et al. 2005. A soft solid surface on Titan as revealed by the Huygens Surface Science Package. *Nature*, **438**, 792–795. doi: 10.1038/nature04211.

Zebker, H. A., Stiles, B., Hensley, S., Lorenz, R., et al. 2009. Size and shape of Saturn's Moon titan. *Science*, **324**, 921–923. doi: 10.1126/science.1168905.

Zebker, Howard A., Wye, Lauren C., Janssen, Michael A., and Team, Cassini Radar. 2008. Titan's surface from reconciled Cassini microwave reflectivity and emissivity observations. *Icarus*, **194**(2), 704 – 710. doi: 10.1016/j.icarus.2007.10.019.